A Numerical Study of the Comparison Between Convectively Forced Hydrostatic and Non-hydrostatic Mesoscale Processes

by

Muhammad Awais
B.Sc., University of the Punjab, 2003
M.Sc., Queen's University, 2010

A Dissertation Submitted in Partial Fulfillment of the
Requirements for the Degree of

DOCTOR OF PHILOSOPHY

in the Department of Mathematics and Statistics

A Numerical Study of the Comparison Between Convectively Forced Hydrostatic and Non-hydrostatic Mesoscale Processes

by

Muhammad Awais
B.Sc., University of the Punjab, 2003
M.Sc., Queen's University, 2010

Supervisory Committee

Dr. S. Ibrahim, Supervisor
(Department of Mathematics and Statistics)

Dr. B. Khouider, Departmental Member
(Department of Mathematics and Statistics)

Dr. A. Monahan, Outside Member
(Department of Earth and Ocean Science)

ABSTRACT

Mesoscale processes in the atmosphere refer to the atmospheric processes that take place within a scale of a few to several hundred kilometres. Atmospheric phenomena like thunderstorms, inertia-gravity waves, jet streaks, fronts and many others have length scales within the range of Mesoscale dynamics. In the study of these processes, because the horizontal length scales are very large as compared to the vertical scales, often vertical acceleration is ignored. Such type of processes are termed as hydrostatic mesoscale processes. If the vertical accelerations are not ignored, then the mesoscale processes are known as nonhydrostatic mesoscale processes. This research work gives a study of the convectively forced nonhydrostatic mesoscale processes. Comparison is made between the results of both hydrostatic and nonhydrostatic mesoscale processes. To do so, a stably stratified, two-dimensional, Boussinesq, nonrotating, inviscid fluid experiencing a thermal forcing is considered under both hydrostatic and nonhydrostatic assumptions. While explicit analytic solutions are available for the hydrostatic cases under both a constant and a shear (linear in z) background profile, to understand the nonhydrostatic cases, a complete discritization of the governing linearized set of equations is carried out for the same background profiles. It has been found that the hydrostatic assumption does not depict the complete dynamics of the process. A horizontal propagation of a wave which is found to be present in the nonhydrostatic cases, is completely missing in the hydrostatic cases.

Further, we show that for both, hydrostatic and nonhydrostatic, cases a sinusoidal shear background profile is nonlinearly unstable. However, because of mathematical difficulties, this work is done for a more specific convectively forced mesoscale processes. More specifically, a sinusoidal background profile is chosen and the external forcing is also treated in a more specific manner. Different from the study of flows forced by an external heating source, where the impacts of the forced wave modes with the atmosphere are studied, for various processes we need to allow the feedback of the atmosphere to the latent heating and a well known way to get such a feedback of the atmosphere is to assume that the diabatic heating is everywhere proportional to the vertical velocity. This kind of treatment of the external forcing is appropriate, for instance, for the processes like *moist convection*. Under such an assumption, the heating will respond to the motion of an air parcel. If the parcel rises upward, latent heat will be released and evaporative cooling will be observed if the parcel of air undergoes a downward motion. To prove the nonlinear instability for a sinusoidal

background profile, first the well-posedness of the governing set of nonlinear equations is established. Then, a linear unstable mode is constructed using a method of continued fractions and then finally, following Grenier's idea, it is shown that the constructed linear unstable mode is also nonlinearly unstable.

Contents

List of Figures

Acknowledgements

First and foremost, I would like to express my heartfelt gratitude to my supervisor Dr. Slim Ibrahim. It has been a complete privilege and pleasure to work under his supervision. I truly acknowledge his valuable and perpetual contributions of time, ideas, guidance, support and patience throughout my Ph.D.

My deep appreciations also go out to Dr. Boualem Khouider and Dr. Adam Monahan for their continuous academic help and knowledgeable discussions. Our interactions were pivotal in my understanding of the physical aspects of this work.

I would also like to thank Dr. Belaid Moa for all the technical support and advice that he provided over the past few years. His generous contributions of time and effort to help resolve all the technical issues during the numerical simulations are greatly appreciated.

Last, I am profoundly indebted to my friends and family who have been immensely patient and supportive throughout this time. Special thanks to my father (late), mother, wife and siblings for their perpetual prayers, love and encouragement.

Chapter 1

Introduction

1.1 Mesoscale dynamics

The content of this chapter comes from my project for the graduate course that I did during the course work of Ph.D. For more details, the reader is referred to [1, 2, 3]. Before we go on and explain the details of our work on mesoscale dynamics, let us start by asking ourselves a few question that would help us better understand mesoscale dynamics.

1. **Why do we need scales in the atmosphere?**
   We observe different kind of phenomena in the atmosphere. All these different phenomena differ from each other in their own time of existence and the length scale on which they exist. For example, a thunderstorm would last for a time scale of about 1 hour to 24 hours and on a length scale of 1 km to 20 km. Whereas, for tornadoes we can have different time and length scales. The phenomenon of turbulence would have its own time and length scale. Therefore, considering that there is a wide range of processes that occur in the atmosphere, it looks very natural to define different time and length scales.

2. **What is a 'Synoptic scale'?**
   As the word synoptic itself tells us the meaning 'forming a synopsis', makes it natural to think about synoptic scale as being a scale of general view. In The Glossary of Meteorology of American Mathematical Society 'Synoptic weather observations' are defined as 'A surface weather observation (observations made from a point on the surface of earth), made at periodic times (usually at three-hourly and six-hourly intervals specified by the World Meteorological Organi-

zation)'. Therefore, as Synoptic weather observation give us a general view of the atmosphere, Synoptic scales are used to study atmospheric phenomena that exist on large scales. Their horizontal scale ranges from several hundred kilometres to several thousand kilometres. Now we go back to our original question which is:

3. **What is 'Mesoscale'?**
   The term 'Microscale' is used to refer to phenomena in the atmosphere that occur on a horizontal length scale of few kilometres or less. Mesoscale is loosely speaking the 'middle scale' in the sense that they have the length scale that is smaller than the synoptic scale but larger than the microscale. According to the AMS glossary of meteorology, mesoscale is defined as: 'Pertaining to atmospheric phenomena having horizontal scales ranging from a few to several hundred kilometers, including thunderstorms, squall lines, fronts, precipitation bands in tropical and extratropical cyclones, and topographically generated weather systems such as mountain waves and sea and land breezes.' (http://glossary.ametsoc.org/wiki/Mesoscale). Now the next question that comes to our mind is:

1.2 Waves in mesoscale

Let us now move towards the discussion on waves that are produced in the mesoscale. There are many factors that can cause the generation of waves in mesoscale but the main causes of the generation of the waves are (1) Orography, (2) Moist convection, (3) Instabilities, (4) Nonlinear interactions, and (5) Heating or cooling. We will give a short overview of these wave generating factors.

1. **Waves produced by Orography**
   As there are parts of the world where we have sequences of mountains, hence, there are a lot of important weather phenomena that fall in the category of mesoscale and are caused by the waves produced due to orography. Hence, the study of waves produced by orography, which are also known as mountain waves, has its own importance. Mountain waves are also a form of very well know lee waves.

2. **Waves produced by Moist convection**
   The rising of the air, which we name as convection, is very common in most

parts of the world. During that process, if we have moisture in the air, if a moist air parcel rises above then it looses heat or cools adiabatically. Some water vapors condense to form a cloud. This kind of convection is called Moist convection. Moist convection is also known to be an agent for the production of internal gravity waves.

3. **Waves produced by Instabilities**
   Mesoscale phenomena including air turbulence, squall lines, rainbands, etc. can be produced due to instabilities that exist in mesoscale dynamics. Instabilities including Static instability (arising due to density diffeerence between air parcel and its environment), Kelvin-Helmholtz instability (which arises when a lighter air flows on top of the heavier one), Inertial instability and also possibly Baroclinic instability can all be responsible for the generation of waves in mesoscale.

4. **Nonlinear interactions**
   Nonlinear excitation of Kelvin-Helmholtz waves and nonlinear internal gravity waves generated by subharmonic excitation (process by which new waves are excited by existing waves) are some of the nonlinear interaction mechanisms that can explain the generation of mesoscale gravity waves.

5. **Heating or cooling**
   Now we turn towards our main point of discussion which is the effects that heating plays in the atmosphere and then more specically, the study of the atmospheric phenomena in mesoscale that occur as a result of heating or cooling. This research work also deals with a system under a specific thermal forcing (details to come later in Chapter 3). Let us explain this particular factor, responsible for the generation of gravity waves, in a little bit more detail.

1.3 Flow response to external heating or cooling

First of all let's start our discussion by understanding the process of convection. First question that we can ask ourselves is that where does the convection occur? As we know that there are parts of the world that get a lot of heat from the sun, especially during summer time. So, the answer should be, almost everywhere. The regions close to the equator especially get really hot in summer times. That actually provides a lot

of heat to the surface of the earth and as a result of which the earth releases a lot of heat which warms up the air above it. The warm air then tends to rise above. Similar is the case with water. If the surface below the water starts to release heat, that would warm up the water that is in contact with the surface of earth and then eventually we are going to have a situation where cold water would be sitting on top of the hot water. Now this is going to induct instability into the system (Rayleigh-Taylor instability). So, all of a sudden motion would be set into the fluid. This motion is not because of any external force but arises only because of the instability that was produced due to heating.

Also, in our daily life, moist convection, which is the process of having clouds, is also a result of convection. If the air on the top of the surface of earth which is releasing heat is moist then we are going to have moist convection which eventually might bring the rainfall. Cumulus clouds and Cumulonimbus clouds are examples of convective clouds. Cumulonimbus clouds are usually related to thunderstorms and heavy rain, may be hailing at times. In areas of the earth where we can have intense heat during the summer, storms can be produced due to the heating and then cooling of the surface of the earth. Countries like Indonesia and equatorial Africa, that get intense rainfall, are the areas where deep convection is most common.

The process of convection can also be started by cooling of the air aloft. This can be observed when winds bring cold air on top of a warm surface. Also when the shallow and deep regions are exposed to a uniform rate of surface cooling during night-time, the shallow water cools faster than the deep water. The difference in the cooling rate then produces a horizontal temperature gradient which as a result drives a gravity current. We can think of the same phenomenon happening in converse for the daytime heating. All these real life factors make the study of the effects of surface heating and cooling very important.

The dynamics of sea and land breezes is a very nice example that motivates us towards the study of heat affects. Land and sea breezes are frequently observed as a result of differential heating (gradient in temperature).

Another important daily life example, for which the study of flow response to heating becomes important, are the heat islands. Most of the main cities now a days get significantly warmer than their surroundings. We call this urban heat island. Heat islands can enhance extreme hot weather events.

Up to now, we have been discussing the processes that involve the heating effects at the surface. We can also study the effects of the heating that happens aloft. For

example, in the troposphere and especially in the stratosphere, heat coming from the sun can warm up the lower and upper parts of the troposphere and the stratosphere, respectively, which can cause different changes in the weather systems.
Next we divert our attention towards the mathematical mechanism that we can adopt to study the affects of surface heating or cooling. We can do this by considering a known function to represent heating or cooling of the surface. For example, a heating that is observed to be periodic in time or space can be represented by a periodic function in the corresponding variables like sine or cosine. The phenomenon of sea-breeze circulations, for instance, is related to the heating which behaves as a periodic function at the ground level. Further, the problems of heat island circulations, sea and land breezes, moist convection, and many others can be studied by using the above mentioned approach of a known function.

1.4 Feedback of the atmosphere to the latent heating or cooling

It has been shown, for example in [4], that the presence of moisture in the atmosphere can have a deep effect on the behaviour of the inertia-gravity waves. In case of thermally forced flows [5, 6, 7], the impacts of the forced wave modes with the atmosphere are studied. However, for the processes like *moist convection*, which as explained above can also be a cause of wave generation in mesoscale flows, we need to allow the feedback of the atmosphere to the latent heating and a well known way to incorporate the effects of the moisture is to assume that the diabatic heating is everywhere proportional to the vertical velocity. Under such an assumption, the heating will respond to the motion of an air parcel. If the parcel rises upward, latent heat will be released and evaporative cooling will be observed if the parcel of air undergoes a downward motion.

1.5 Research problem under consideration

Now we are in a position to state the main problem that is studied in this dissertation. Firstly, we would like to study the flow response of a nonhydrostatic atmosphere to an external heating (details to follow in Chapter 3) and the external heating will be

considered to be aloft and impulsive. Secondly, we will show that for the same governing set of equations, a sinusoidal shear background profile is nonlinearly unstable (details to follow in Chapter 4).

However, due to mathematical difficulties, the treatment of the external forcing will be different for this part of the work. As the idea in this section will be to start with an *ansatz* and then try to look for an unstable mode, the main difficulty arises when we try to insert the *ansatz* into the governing set of equations that we have. More specifically, the external forcing function that we will consider in the first part of the thesis will be singular in both time and space (only the $z-$variable) and therefore, for example, if we begin with a wave-type solution, the forcing function will get in our way as it will not have the form of the solution that we are trying to enforce. Now, to overcome this problem, we consider a more specific atmosphere. We will be assuming that the external forcing function is everywhere out of phase with the vertical velocity. This type of treatment of the forcing function is more relevant when the response of the atmosphere to any kind of motion also becomes important. So, as opposed to the first part of the thesis where we will force the atmosphere with an external heating source and then try to look at the behaviour of the forced waves, in the later part of the thesis, to overcome some mathematical problems, that we face for the construction of a linear unstable mode in Chapter 3, section 3.2, we will consider the external heating to be dependent on the vertical velocity.

1.6 Organization of the dissertation

The current chapter serves as an introduction and to motivate the importance of the problem under consideration. The dissertation from here onwards is organized as follows:

Chapter 2 provides us with a detailed introduction to the governing set of equations and then an overview of the mathematical set up of the problem. It further provides us with the details of the numerical scheme used and the results of the problem of flow response to the external heating, first, under a uniform background and then, secondly, under a shear dependent background profile. **Chapter 3** includes a review of the necessary condition for instability, the method and details of the construction of a linear unstable mode along with a few additional examples of linear unstable background profiles. In **Chapter 4** we further extend the work of Chapter 3 and show that the previously constructed linear unstable mode is also unstable in the

nonlinear sense. **Chapter 5** includes the details of the numerical methods that performed poorly in the process of doing simulations.

Chapter 2

Flow Response to the Impulse Heating or Cooling

2.1 Literature Review

Our main point of focus here is to study the effects of heating sources in the dynamics of mesoscale flows under both hydrostatic and nonhydrostatic conditions. These kind of problems have previously been considered as well. Han and Baik (2008) [5] theoretically investigated the transient response of a nonrotating, stably stratified, boussinesq, hydrostatic and uniform atmosphere to a convective singular forcing in 3D. Using the explicit analytic solutions that were obtained using the Fourier and the Laplace transforms, the flow response to the surface pulse heating was found to be axisymmetric with respect to the moving axis that moves downwind with the speed of the uniform background wind. Also, the vertical displacement at the centre of the steady heating was explicitly shown to decay as t^{-1} for large t. The effects of the same convective singular forcing under a shear dependent background profile were investigated in 2D by Baik, Hwang and Chun (1998) [6] and later in 3D by Han and Baik (2009) [7]. In [6], the governing set of equations were solved analytically and it was shown that in case of point pulse forcing there is only one critical level and the attenuation factor for internal gravity waves that pass through the critical level depends only on the Richardson number. However, for the case of line type pulse forcing, there are infinite number of critical levels and the attenuation factor is spatially dependent, both in time and space. In [7], the same problem was extended to 3D and another theoretical study was carried out by finding exact analytic solutions. Under surface

pulse heating, near the centre of the moving mode, it was noticed that the magnitude of the vertical velocity became constant after some time, whereas the magnitudes of the vertical displacement and perturbation horizontal velocity were observed to increase linearly with time. More recently, using a similar non-dimensional numerical model, Han and Baik (2012) [8] provided us with an insight into the nonlinear effects on convectively forced two-dimensional mesoscale flows. According to their results, even in the absence of vertical wind shear (i.e. constant background), nonlinearity causes a separation of an upwind cellular draft from the steady-heating induced main up-draft and increasing the strength of the nonlinearity also increases the strength of the separated upwind cellular draft. However, all these studies mentioned above made a very strong and vital assumption of hydrostatic balance. It is assumed that in comparison to horizontal accelerations, the vertical acceleration is negligible ($\frac{Dw}{Dt} = 0$). Regarding nonhydrostatic studies, in order to validate their numerical scheme, Moustoui, Joseph and Teitelbaum in (2004) [9] used the non-hydrostatic set of equations experiencing a thermal forcing, which is bell-shapped in the horizontal and sinusoidal up to a height and zero from there onwards. Analytic solution of the problem was derived to make a comparison with the numerical solution. However, in terms of a comparison between hydrostatic and nonhydrostatic cases, the earliest such comparison was made by Queney [10] where the linearized, steady-state equations for an atmosphere with constant wind and stability were considered. According to his work, the vertical acceleration is negligible for a topography with half width greater than about 10 Km. More recentely, Teddie L. Keller [11] made a comparison of hydrostatic and nonhydrostatic solutions of linear two dimensional steady state flow under topographic forcing to make a clear conclusion that hydrostatic assumption alters the results significantly. More specifically, it was noticed that for 'troposhere-only' atmospheric model (the wind increases linearly with height to infinity and the stability is constant), all waves present were always trapped for the nonhydrostatic case. However, the hydrostatic assumption completely abolished the trapped modes and therefore, even for a relatively large-scale topographic forcing, the nonhydrostatic affects may still be very important.

So, for this chapter, our way forward from here on is first to recall the governing equations for general (hydrostatic and nonhydrostatic) mesoscale processes experiencing a heating source and then secondly apply an appropriate numerical method to solve the governing nondimensional set of equations. Because the characteristics of gravity waves produced in the atmosphere depend very strongly on the basic state

wind, we will consider two different cases for the basic state wind here: (1) Uniform basic state wind and (2) Shear dependent basic state wind. Contours of hydrostatic and nonhydrostatic perturbation vertical velocities, for both cases of basic state wind, will be presented at the end to depict the difference in behaviours.

2.2 Governing equations

Governing equations for mesoscale dynamics include the equation for coservation of momentum, conservation of mass and the thermodynamic energy equation [1], respectively, given as

$$\frac{DU}{Dt} + JU = -\frac{1}{\rho}\nabla p + (0, 0, -g)^{T_r} + F_r, \tag{2.1}$$

$$\frac{D\rho}{Dt} + \rho(\nabla.U) = 0, \tag{2.2}$$

$$\frac{D\theta}{Dt} = \frac{\theta}{c_p T} q, \tag{2.3}$$

In order to close the system, we use the equation of state

$$S\left(p, \rho, T\right) = 0, \tag{2.4}$$

which, for example, for dry air becomes $p = \rho R_d T$ and Poisson's equation

$$\theta = T(\frac{p_s}{p})^{\frac{R_d}{c_p}}. \tag{2.5}$$

Here Equation (2.1) is known as the momentum equations which for the case of zero coriolis ($f = 0$) are often called Euler equations in literature. Equation (2.2) is the continuity equation and the equation (2.3) is the thermodynamic energy equation. The symbol $U\left(\mathbf{x}, t\right)$ stands for the velocity vector given as $U\left(\mathbf{x}, t\right) = \left(u\left(\mathbf{x}, t\right), v\left(\mathbf{x}, t\right), w\left(\mathbf{x}, t\right)\right)$ and the symbol $\frac{D}{Dt}$ is the material derivative given by $\frac{D}{Dt} = \frac{\partial}{\partial t} + (U.\nabla)$, R_d is the gas constant for dry air, $\theta\left(\mathbf{x}, t\right)$ is the potential temperature, $q\left(\mathbf{x}, t\right)$ is the heating rate, ρ is the density, $p\left(\mathbf{x}, t\right)$ is the pressure, F_r represents frictional forces and f is the

Coriolis parameter and the matrix J is given by

$$J = \begin{pmatrix} 0 & -f & 0 \\ f & 0 & 0 \\ 0 & 0 & 0 \end{pmatrix} \tag{2.6}$$

2.2.1 Linearization of Equations $(2.1) - (2.3)$

We linearize equations $(2.1)-(2.3)$ around the basic state $(U_{stat}(z), \rho_{stat}(z), \theta_{stat}(z), p_{stat}(z))$, i.e., we consider

$$\begin{aligned} U(\mathbf{x},t) &= U'(\mathbf{x},t) + U_{stat}(z), && (2.7)\\ p(\mathbf{x},t) &= p'(\mathbf{x},t) + p_{stat}(z), && (2.8)\\ \theta(\mathbf{x},t) &= \theta'(\mathbf{x},t) + \theta_{stat}(z), && (2.9)\\ \rho(\mathbf{x},t) &= \rho'(\mathbf{x},t) + \rho_{stat}(z), && (2.10)\\ T(\mathbf{x},t) &= T'(\mathbf{x},t) + T_{stat}(z), && (2.11)\\ q(\mathbf{x},t) &= q'(\mathbf{x},t), && (2.12) \end{aligned}$$

where the notation prime denotes the perturbation in the respective quantity and the subscript '*stat*' represent the basic state. Considering a velocity field of the form $U_{stat}(z) = (u_{stat}(z), v_{stat}(z), 0)$ in (2.1) gives us the following equilibrium equations:

1. **Geostrophic Wind Balance:**

$$u_{stat}(z) = -\frac{1}{f\rho_{stat}}\frac{\partial p_{stat}}{\partial y}, \quad v_{stat}(z) = \frac{1}{f\rho_{stat}}\frac{\partial p_{stat}}{\partial x}, \tag{2.13}$$

2. **Hydrostatic Balance:**

$$\frac{\partial p_{stat}}{\partial z} = -g\rho_{stat}, \tag{2.14}$$

Using equations (2.13) and (2.14), one gets the so called **Thermal Wind Balance**, given as:

$$\frac{du_{stat}}{dz} = -\frac{g}{f\theta_{stat}}\frac{\partial \theta_{stat}}{\partial y}, \quad \frac{dv_{stat}}{dz} = \frac{g}{f\theta_{stat}}\frac{\partial \theta_{stat}}{\partial x}, \tag{2.15}$$

The Conservation of basic state thermal wind energy is given as:

$$u_{stat}\frac{\partial \theta_{stat}}{\partial x} + v_{stat}\frac{\partial \theta_{stat}}{\partial y} = 0. \tag{2.16}$$

Using equations $(2.7) - (2.12)$ in equations $(2.1) - (2.3)$ and neglecting the nonlinear terms gives us the set of linearized equations given by (for convenience dropping the prime notation)

$$\frac{D_{stat}U}{Dt} + JU + w\frac{dU_{stat}}{dz} = -\nabla\pi + \hat{e}_3 b + F_r, \tag{2.17}$$

$$\frac{D_{stat}b}{Dt} + f\left(\frac{dv_{stat}}{dz}u - \frac{du_{stat}}{dz}v\right) + N^2 w = \frac{g}{c_p T_{stat}}q, \tag{2.18}$$

$$\nabla.U = 0, \tag{2.19}$$

where $N^2 = \frac{g}{\theta_{stat}}\frac{d\theta_{stat}}{dz}$ is the Brunt-Vaisala frequency, $b = \frac{g\theta}{\theta_{stat}}$, $\pi = \frac{p}{\rho_{stat}}$, $\hat{e}_3$ is a unit vector along $z-$axis and the symbol $\frac{D_{stat}}{Dt}$ represents $\frac{D_{stat}}{Dt} = \frac{\partial}{\partial t} + (U_{stat}\cdot\nabla)$.
Considering a flow to be incompressible, two-dimensional (no dependence on y and taking $v(\mathbf{x}, t) \equiv 0$), nonrotating, ignoring the frictional forces and taking into account the boussinesq approximations (density is considered as a constant ρ_0 except where it is coupled with gravity), equations $(2.17) - (2.19)$ can be written as

$$\frac{\partial u}{\partial t} + u_{stat}\frac{\partial u}{\partial x} + w\frac{du_{stat}}{dz} = -\frac{\partial \pi}{\partial x}, \tag{2.20}$$

$$\frac{\partial w}{\partial t} + u_{stat}\frac{\partial w}{\partial x} = -\frac{\partial \pi}{\partial z} + b, \tag{2.21}$$

$$\frac{\partial b}{\partial t} + u_{stat}\frac{\partial b}{\partial x} + N^2 w = \frac{g}{c_p T_{stat}}q, \tag{2.22}$$

$$\frac{\partial u}{\partial x} + \frac{\partial w}{\partial z} = 0. \tag{2.23}$$

Here $u(t, x, z)$ and $w(t, x, z)$ are the two components of velocity, $\pi(t, x, z)$ is the pressure, $b(t, x, z)$ is the potential temperature and $q(t, x, z)$ is the thermal focing. Equations (2.20) and (2.21) define the momentum equation, while the identity (2.22) is the thermodynamic energy equation and equation (2.23) is the continuity equation.
Consider the following non-dimensionalization [8]

$$t' = \frac{u_c}{L}t, \quad x' = \frac{x}{L}, \quad z' = \frac{N}{u_c}z, \quad u'_{stat} = \frac{u_{stat}}{u_c}, \quad \alpha' = \frac{\alpha}{N}, \quad q' = \frac{q}{q_0},$$
$$u' = \frac{c_p T_0 N u_c}{g q_0 L}u, \quad w' = \frac{c_p T_0 N^2}{g q_0}w, \quad \pi' = \frac{c_p T_0 N}{g q_0 L}\pi, \quad b' = \frac{c_p T_0 u_c}{g q_0 L}b$$

where L and u_c are characteristic length and velocity scales, respectively. These characteristic quantities depend upon each specific problem. In new coordinates, equations $(2.20) - (2.23)$ become (after removing the primes)

$$\frac{\partial u}{\partial t} + u_{stat}\frac{\partial u}{\partial x} + w\frac{du_{stat}}{dz} = -\frac{\partial \pi}{\partial x} \tag{2.24}$$

$$\varepsilon^2\left[\frac{\partial w}{\partial t} + u_{stat}\frac{\partial w}{\partial x}\right] = -\frac{\partial \pi}{\partial z} + b \tag{2.25}$$

$$\frac{\partial b}{\partial t} + u_{stat}\frac{\partial b}{\partial x} + w = q \tag{2.26}$$

$$\frac{\partial u}{\partial x} + \frac{\partial w}{\partial z} = 0, \tag{2.27}$$

where $\varepsilon = u_c/LN$ is a small parameter with $0 < \varepsilon < 1$. The limit $\lim_{\varepsilon \to 0}$ takes us to the hydrostatic case which corresponds to much larger horizontal length scale as compared to the vertical scales. This limit is also comparable to taking the long-wavelength limit of the governing dynamics of the considered mesoscale flow. Taking an $x-$derivative of equation (2.24) and $z-$derivative of equation (2.25) and then adding them together gives us the following Poisson's equation

$$\frac{\partial^2 \pi}{\partial x^2} + \frac{1}{\varepsilon^2}\frac{\partial^2 \pi}{\partial z^2} = \frac{1}{\varepsilon^2}\frac{\partial b}{\partial z} - 2\frac{\partial w}{\partial x}\frac{d\tilde{u}}{dz} \tag{2.28}$$

Note that, following the same procedure as done above for linearization, the non-linear system $(2.1) - (2.3)$ can also be written as [8]

$$\frac{\partial u}{\partial t} + u_{stat}\frac{\partial u}{\partial x} + w\frac{du_{stat}}{dz} = -\frac{\partial \pi}{\partial x} - \phi\left(u\frac{\partial u}{\partial x} + w\frac{\partial u}{\partial z}\right), \tag{2.29}$$

$$\varepsilon^2\left[\frac{\partial w}{\partial t} + u_{stat}\frac{\partial w}{\partial x}\right] = -\frac{\partial \pi}{\partial z} + b - \left(\varepsilon^2\phi\right)\left(u\frac{\partial w}{\partial x} + w\frac{\partial w}{\partial z}\right), \tag{2.30}$$

$$\frac{\partial b}{\partial t} + u_{stat}\frac{\partial b}{\partial x} + w = q - \phi\left(u\frac{\partial b}{\partial x} + w\frac{\partial b}{\partial z}\right), \tag{2.31}$$

$$\frac{\partial u}{\partial x} + \frac{\partial w}{\partial z} = 0. \tag{2.32}$$

and

$$\varepsilon^2\frac{\partial^2 \pi}{\partial x^2} + \frac{\partial^2 \pi}{\partial z^2} = 2\varepsilon^2\phi\left(\frac{\partial u}{\partial x}\frac{\partial w}{\partial z} - \frac{\partial w}{\partial x}\frac{\partial u}{\partial z}\right) + \frac{\partial b}{\partial z} - 2\varepsilon^2\frac{\partial w}{\partial x}\frac{du_{stat}}{dz} \tag{2.33}$$

with $\phi = gq_0L/c_pT_0Nu_0^2$ will determine the strength of the nonlinearity. As pointed out by Keller in [11], the nonlinearities may enhance the excitation and the amplitude of the nonhydrostatic modes, so, in order to isolate the nonlinear effects from the nonhydrostatic ones, we will first consider the system $(2.24 - 2.28)$ and then later we will consider the system $(2.29 - 2.33)$. The domain will be taken as infinite in the $x-$direction and either semi-infinite or bounded between two rigid layers located at $z = z_1, z_2$ in the $z-$ direction, i.e., either $\Omega = (-\infty, \infty) \times (0, \infty)$ or $\Omega = (-\infty, \infty) \times (z_1, z_2)$. In case of semi-infinite domain, we will consider a flat bottom boundary condition ($w(t, x, z) = 0$ at $z = 0$) and the upper radiation boundary condition ($w(t, x, z)$ is finite at $z = \infty$). Whereas, in the later case, we will consider $w(t, x, z) = 0$, both at $z = z_1$ and $z = z_2$.

2.3 Numerics

Equations (2.24)-(2.27) will be solved by using the method described in [12]. This method uses the filtered Leapfrog scheme in time to solve an evolution equation of the form

$$\frac{\partial \psi}{\partial t} = f(\psi)$$

and has the form

$$\frac{\psi^{n+1} - \bar{\psi}^{n-1}}{2\nabla t} = F(\psi^n)$$

with

$$\bar{\psi}^{n-1} = \psi^{n-1} + \gamma_4 \left(-\bar{\psi}^{n-3} + 4\bar{\psi}^{n-2} - 6\bar{\psi}^{n-1} + 4\psi^n - \psi^{n+1}\right)$$

where $\bar{\psi}^n$ is the solution after applying a fourth-order implicit time filter and γ is a constant that determines the strength of the filter. Letting

$$\tilde{\psi}^{n-1} = \psi^{n-1} + \gamma_4 \left(-\bar{\psi}^{n-3} + 4\bar{\psi}^{n-2} - 4\psi^n\right)$$

the recursion formula for the above mentioned scheme can be formulated as

$$\bar{\psi}^{n-1} = \frac{-2\Delta t\gamma f(\psi^n) + \tilde{\psi}^{n-1}}{1+7\gamma} \tag{2.34}$$

$$\psi^{n+1} = \frac{2(1+6\gamma)\Delta t f(\psi^n) + \tilde{\psi}^{n-1}}{1+7\gamma} \tag{2.35}$$

$$\tilde{\psi}^n = \psi^n + \gamma\left(-\bar{\psi}^{n-2} + 4\bar{\psi}^{n-1} + 4\psi^{n+1}\right) \tag{2.36}$$

The computational domain will be considered to be about 1000 Km in the horizontal direction (with a uniform grid spacing of 4 Km) and about 40 Km in the vertical direction (with a uniform grid spacing of 150 meters).
Periodic boundary condition in the horizontal direction will be considered and, as already mentioned, the domain is considered wide enough such that the dynamics takes place within the considered spatial domain. At the zero level in the vertical, a flat bottom boundary condition will be used. Also, at the upper level, the solutions will be considered zero as well.

2.3.1 Validation of the numerical code

In order to validate our numerical code, we consider the streamfunction-vorticity formulation of the system of equations (2.20)-(2.23), as it was done in [9]

$$\left(\frac{\partial}{\partial t} + u_{stat}\frac{\partial}{\partial x}\right)\eta + \frac{\partial b}{\partial x} = 0, \tag{2.37}$$

$$\left(\frac{\partial}{\partial t} + u_{stat}\frac{\partial}{\partial x}\right)b - N^2\frac{\partial \psi}{\partial x} = q = Q_0 f(x,z)g(t), \tag{2.38}$$

$$\left(\frac{\partial^2}{\partial x^2} + \frac{\partial^2}{\partial z^2}\right)\psi = \eta. \tag{2.39}$$

where $u = \partial\psi/\partial z, w = -\partial\psi/\partial x$ and $\eta = \partial u/\partial z - \partial w/\partial x$. The exact solution to the above system (2.37)-(2.39) is found in [9] by expanding the variables in the form

$$\beta(t,x,z) = \sum_{k,m} \beta_{km}(t)e^{ikx}\sin(mz), \tag{2.40}$$

with $k = (2\pi/L)p, m = (\pi/H)q$ with p and q being integers. The coefficients of the vertical velocity with $\tilde{u} = 0, g(t) = (1/2)(1 - \cos\omega_0 t)$ and

$$f(x,z) = \begin{cases} \frac{\sin(\pi z/L_z)}{1+x^2/L_x^2} & \text{for} \quad z \le L_z \\ \\ 0 & \text{for} \quad z \ge L_z \end{cases}, \tag{2.41}$$

are given by

$$w_{km}(t) = \frac{Q_0 f_{km}}{2N^2}\left[(1-\cos\omega t) + \frac{\omega^2}{\omega_0^2-\omega^2}\left(\cos\omega_0 t - \cos\omega t\right)\right], \tag{2.42}$$

where $\omega_0 = 2\pi/T_0$ and $\omega = \sqrt{k^2N^2/(k^2+m^2)}$. Now consider the following plots.

(a) **Exact Solution** (b) **Numerical Solution**

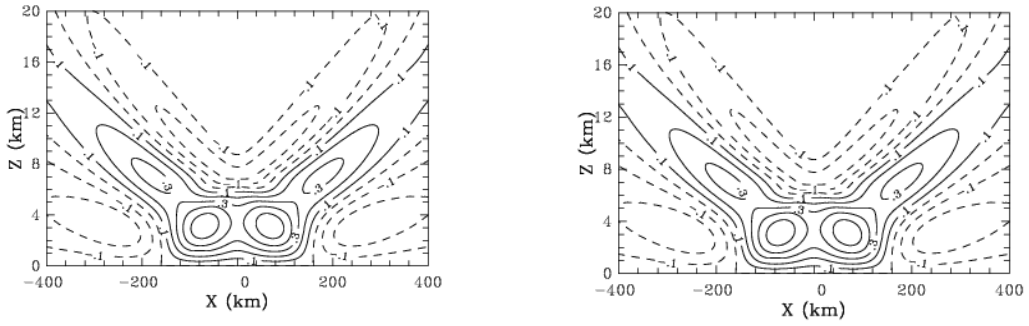

Figure 2.1: Contours for the perturbation vertical velocity at 2 hours using (a) Analytic solution and (b) Numerically. Values of the parameters used are $T_0 = 2$ h, $L_x = 30$ Km, $L_z = 8$ Km, $Q_0 = 0.001$ ms^{-3}, and $N^2 = 4 \times 10^{-}4$ s^{-2}.

From here onwards, we will consider the diabatic forcing $q(t,x,z)$ in (2.22) and (2.26) to have the following form

$$q(t,x,z) = q_0 \frac{a^2}{a^2+x^2}\delta(t)\delta(z-h), \tag{2.43}$$

with q_0 being the amplitude of the thermal forcing, a being the half width of the bell-

shaped function, δ being the Dirac delta distribution, and h represents the height at which the heat pulse will be released. Regarding the hydrostatic case, we give a short review of the work in [5]-[8]. Taking $\varepsilon = 0$ and applying the Fourier transform in $(x \to k)$ and the Laplace transform in $(t \to s)$, equations (2.20)-(2.23) can be reduced to a single equation in the transformed perturbation vertical velocity $\hat{w}(s, k, z)$, given by

$$\frac{\partial^2 \hat{w}}{\partial z^2} - \frac{k^2 N^2}{(s + iku_{stat})^2}\hat{w} = -\frac{gq_0 k^2 a e^{-ak}\delta(z-h)}{c_p T_0 (s + iku_{stat}(h))^2}, \tag{2.44}$$

where $u_{stat}(h)$ represents the background $u_{stat}(z)$ evaluated at $z = h$. The above equation (2.44) is first solved using:
Upper radition condition:

$$\hat{w}_2(k, z, s) \text{ is finite at } z = \infty \tag{2.45}$$

Flat bottom condition:

$$\hat{w}_1(k, z, s) \;=\; 0 \text{ at } z = 0, \tag{2.46}$$

and two interface conditions at $z = h$, given by

$$\frac{\partial \hat{w}_2}{\partial z} - \frac{\partial \hat{w}_1}{\partial z} \;=\; \frac{gq_0 a (ik)^2 e^{-ak}}{c_p T_0 (s + iku_{stat}(h))^2}, \tag{2.47}$$

$$\hat{w}_2 - \hat{w}_1 \;=\; 0, \tag{2.48}$$

and then the solutions are transformed back into the original space by carrying out the inverse Laplace and the Fourier transforms under both a uniform and a shear dependent background profile. For details the reader is referred to [5]-[8]. Now, in order to solve the nonhydrostatic ($\varepsilon = 1$) set of equations (2.24)-(2.27), we implement the numerical scheme introduced in section-2.3 above. Also, for the purpose of numerical computing, we will be approximating the dirac delta distribution $\delta(y)$ using

$$\delta(y) = \lim_{\epsilon \to 0} \frac{1}{\pi} \frac{\epsilon}{y^2 + \epsilon^2}. \tag{2.49}$$

Now we move towards presenting the graphical results for both hydrostatic and non-hydrostatic cases each first considered under a uniform and then a shear background profile.

2.3.2 Uniform Background

Here we take the background profile to be constant with height, i.e., $\tilde{u}(z) = U_0$. Consider the following plots for the hydrostatic case, produced using the exact solution from [5].

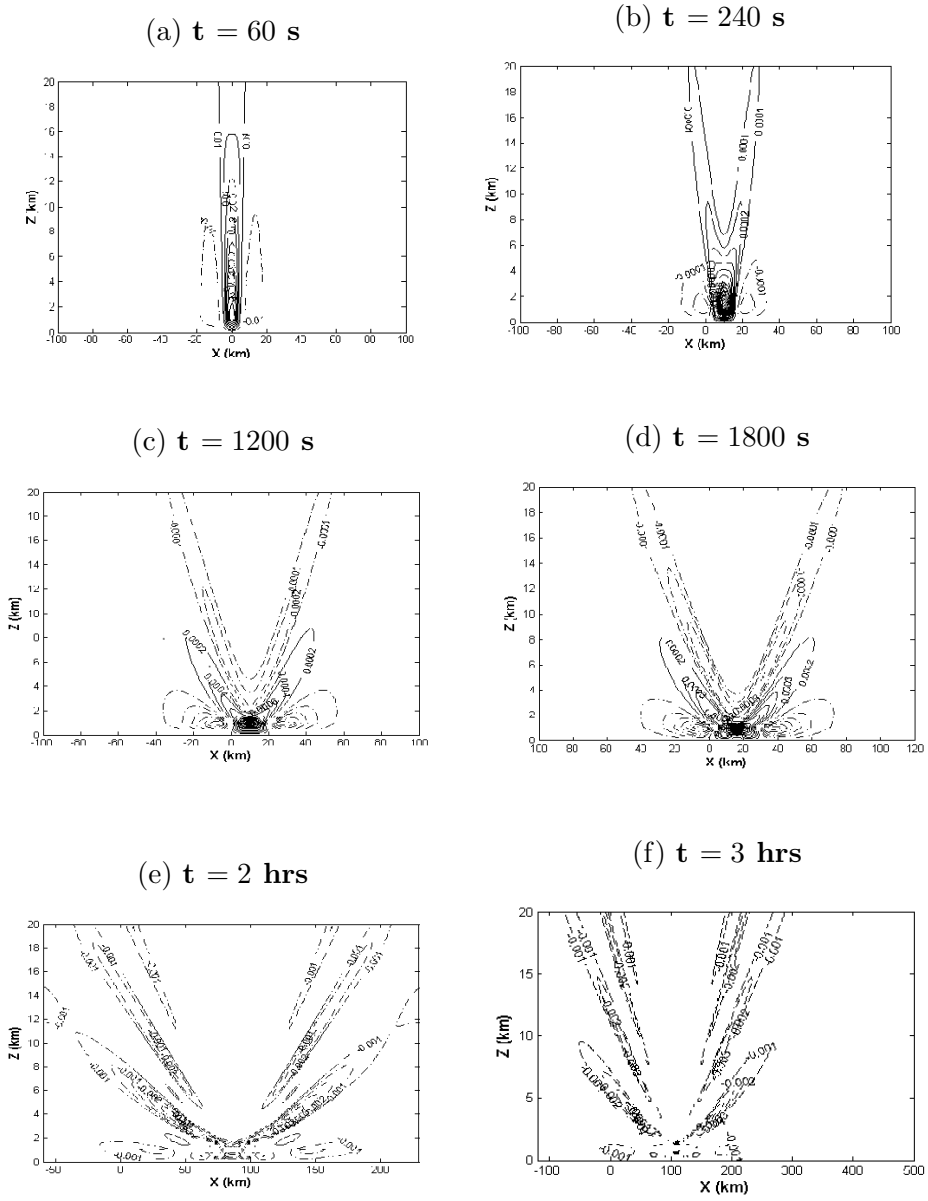

Figure 2.2: Contours for the time evolution of the hydrostatic perturbation vertical velocity under a uniform background profile.

The following contours for the nonhydrostatic perturbation vertical velocity are produced by numerically solving the governing set of equations (2.24)-(2.27).

(a) $\mathbf{t} = 60$ **s**

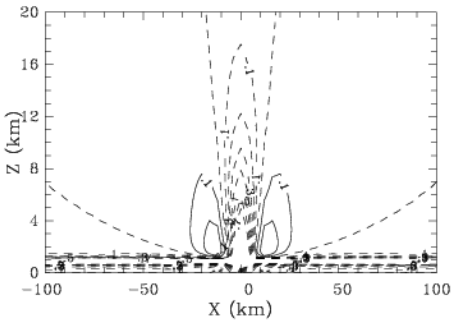

(b) $\mathbf{t} = 240$ **s**

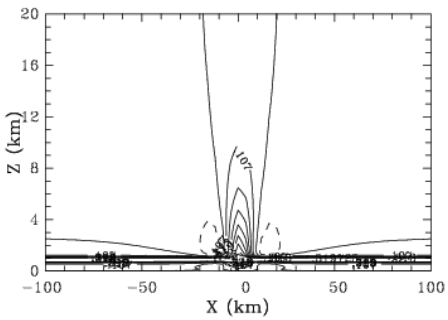

(c) $\mathbf{t} = 1200$ **s**

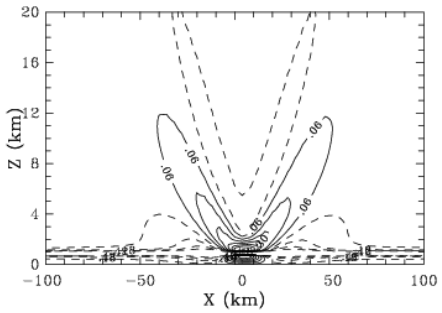

(d) $\mathbf{t} = 1800$ **s**

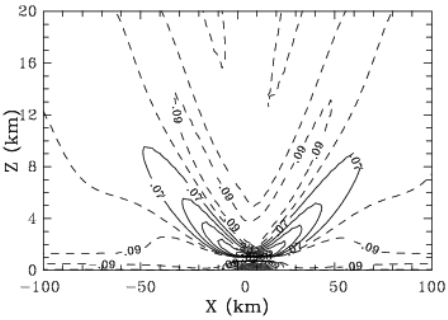

(e) $\mathbf{t} = 2$ **hrs**

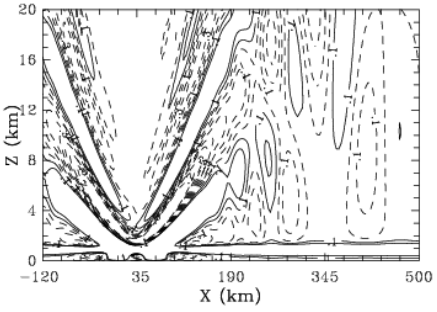

(f) $\mathbf{t} = 3$ **hrs**

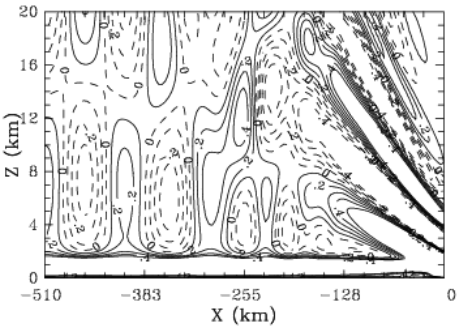

Figure 2.3: Contours for the time evolution of the nonhydrostatic perturbation vertical velocity under a uniform background profile.

2.3.3 Shear Background

As a second case now, we take the background profile to increase linearly to infinity with height, i.e., $\tilde{u}(z) = -\alpha z$. Consider the following plots for the hydrostatic case, again produced using the exact solution from [6].

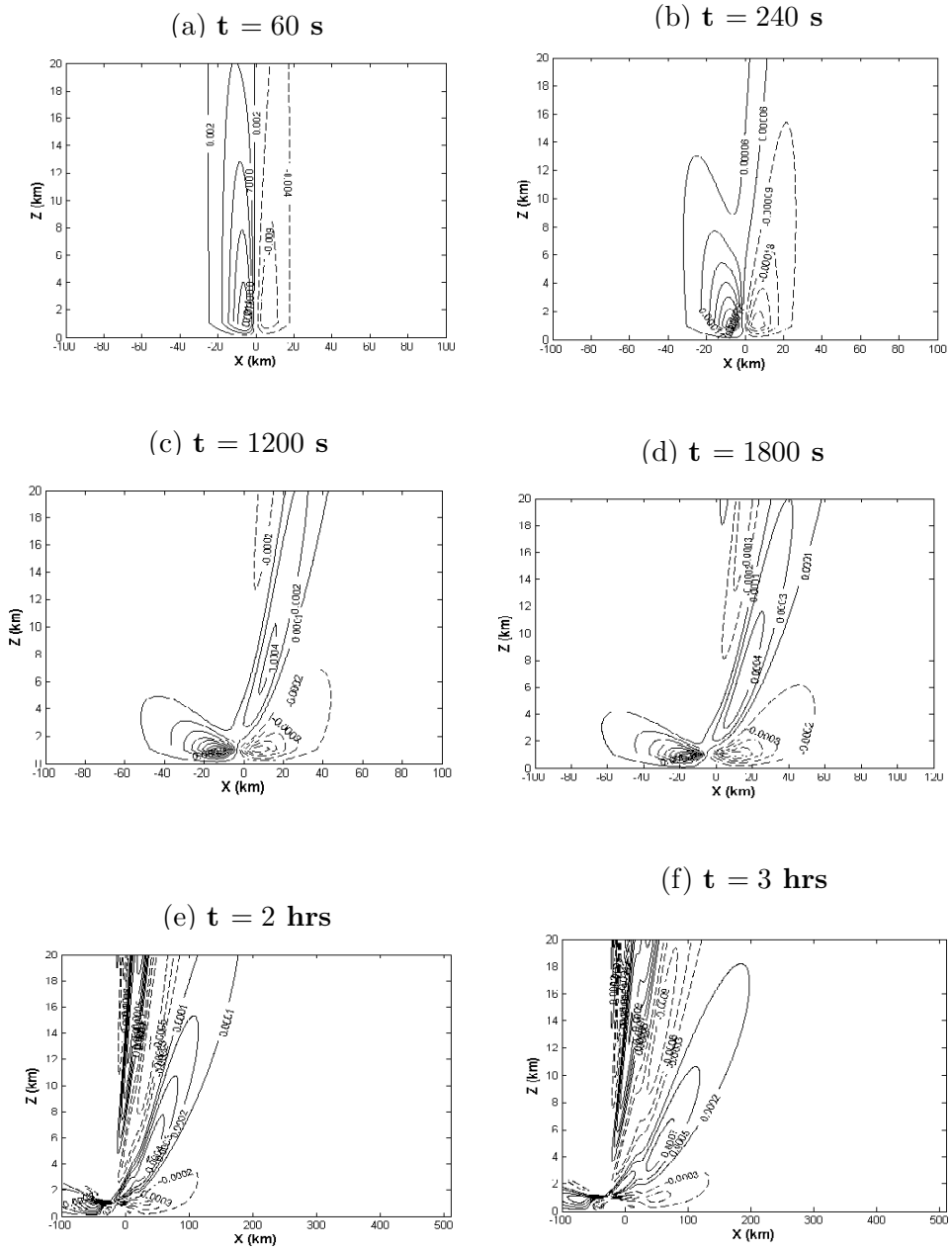

Figure 2.4: Contours for the time evolution of the hydrostatic perturbation vertical velocity under a shear background profile.

Lastly, we present the following contours for the nonhydrostatic perturbation vertical velocity produced by numerically solving the governing set of equations (2.24)-(2.27).

(a) $\mathbf{t} = 60$ **s**

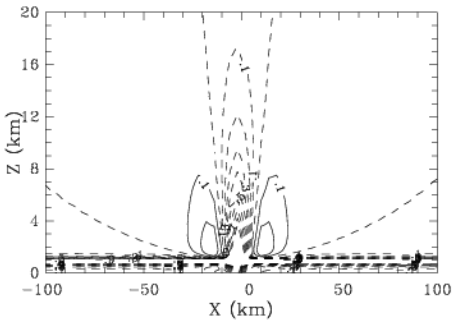

(b) $\mathbf{t} = 240$ **s**

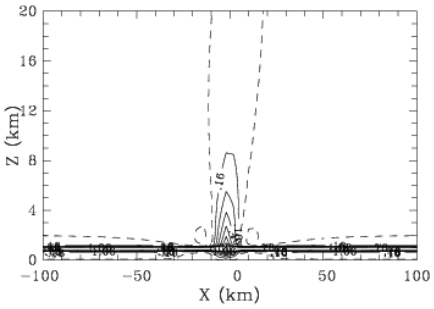

(c) $\mathbf{t} = 1200$ **s**

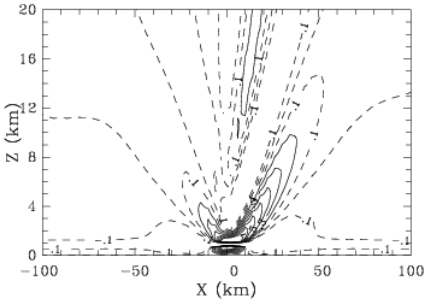

(d) $\mathbf{t} = 1800$ **s**

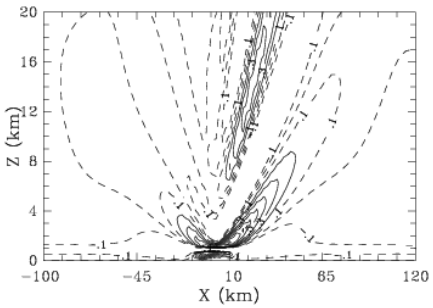

(e) $\mathbf{t} = 2$ **hrs**

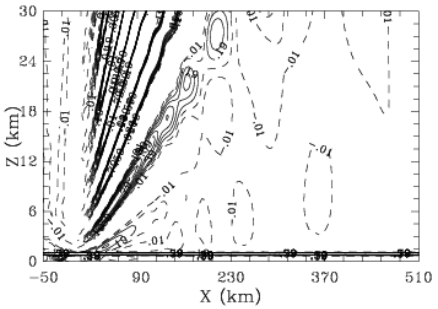

(f) $\mathbf{t} = 3$ **hrs**

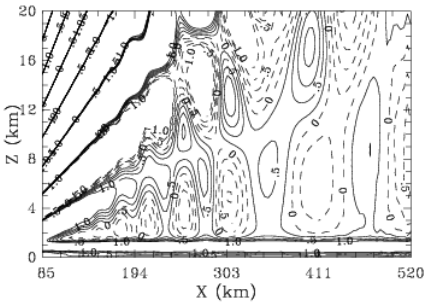

Figure 2.5: Contours for the time evolution of the nonhydrostatic perturbation vertical velocity under a shear background profile.

2.4 Discussion and Conclusion

Values of the parameters used to make the contour plots are given by: $U_0 = 10$ ms^{-1}, $N^2 = 4 \times 10^{-4}$ s^{-2}, $\alpha = 0.0025$ s^{-1}, $a = 10$ Km and the heating pulse is released at the height $h = 1$ Km. Contours for the perturbation vertical velocity with uniform background for the hydrostatic case are depicted in figure-2.2 and for the nonhydrostatic case are shown in figure-2.3. The contours presented are first rescaled in each case. For figures (2.2)-(2.3), subplots (a) and (f) are rescaled by 10^5 and the remaining are rescaled by 10^4. Whereas, for figures (2.4)-(2.5), plots in subfigures (a) and (f) are rescaled by 10^5 and all others are rescaled by 10^3.

Comparing the behaviour of the hydrostatic and nonhydrostatic cases under constant background, we can see a similarity in the behaviour for short values of time. For example, after $t = 240$ s, in both figure-(2.2b) and figure-(2.3b), the main upward moving mode that appears at the point where the heating pulse is applied gets advected downwind with a compensating downward motion of the air appearing around it. Also, the symmetry in the behaviour around a vertical line that passes through the centre of the main moving mode is preserved for the nonhydrostatic case as well. However, as the time progresses, the hydrostatic and nonhydrostatic cases start to differ from each other. The symmetry of the contours for the nonhydrostatic case disappears as time progresses. For large values of time, the difference in the behaviour between the two cases becomes more and more evident. A horizontal propagation of the wave which clearly exists in the nonhydrostatic case, as shown in figures (2.4e) and (2.4f), is completely absent in the hydrostatic case. A similar behaviour in case of nonhydrostatic atmosphere was also observed by Keller [11].

Moving to the case of shear background, the contours for the hydrostatic and nonhydrostatic cases are presented in figure-2.4 and figure-2.5. As is the case of uniform background, a straight upright vertical motion is observed at the start which later starts to tilt and develops a slope as the time progresses and this behaviour is observed both for the hydrostatic and the nonhydrostatic flows. However, in the presence of the shear, the hydrostatic and nonhydrostatic cases behave very differently for large values of time again. Similar to the case of uniform background, with shear background profile, regions of positive and negative modes in the horizontal direction are observed for the nonhydrostatic case. These modes are completely wiped out by the hydrostatic assumption though.

Next, we try to make sure that the differences between the hydrostatic and nonhy-

drostatic cases pointed above are not caused by the reflections from the top of the domain. To do so, we consider a 5 Km deep absorbing layer of Rayleigh friction starting from about 35 Km and extending up to the upper end of the domain which is taken as 40 Km. Consider the following plots now:

(a) **t = 2 hours** (b) **t = 3 hours**

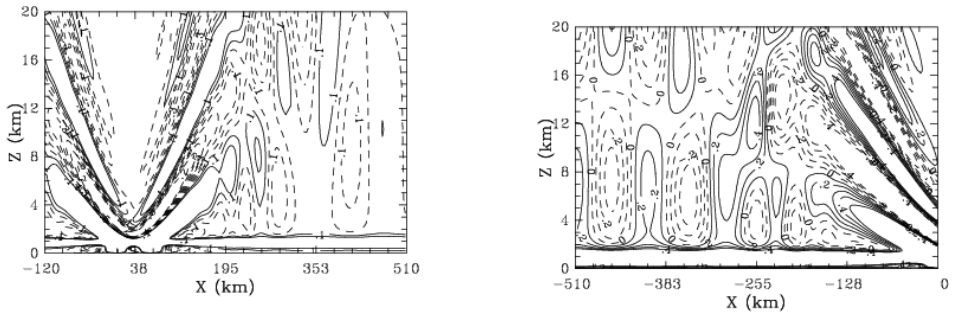

Figure 2.6: Contours for the nonhydrostatic perturbation vertical velocity under a uniform background profile at (a) $t = 2$ hours, (b) $t = 3$ hours.

(a) **t = 2 hours** (b) **t = 3 hours**

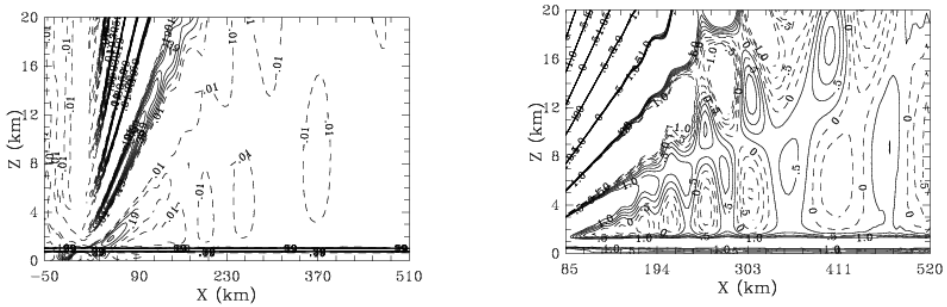

Figure 2.7: Contours for the nonhydrostatic perturbation vertical velocity under a shear background profile at (a) $t = 2$ hours, (b) $t = 3$ hours.

Figures (2.6) and (2.7) show the behaviour of the nonhydrostatic perturbation vertical velocity at $t = 2$ and $t = 3$ hours under a constant and a shear background profile, respectively, plotted using a sponge layer at the top of the domain to minimize the reflections from the upper end of the boundary. Horizontally propagating regions of upward and downward motions that were observed earlier in figures (2.3) and (2.5) for the same values of time are still present.

Finally, we turn towards the inclusion of nonlinearities into the atmosphere by using the system of equations $(2.29 - 2.33)$. We keep the same boundary conditions as before and a similar sponge layer of Rayleigh friction is also applied.

(a) **t** = 1800 **seconds** (b) **t** = 1800 **seconds**

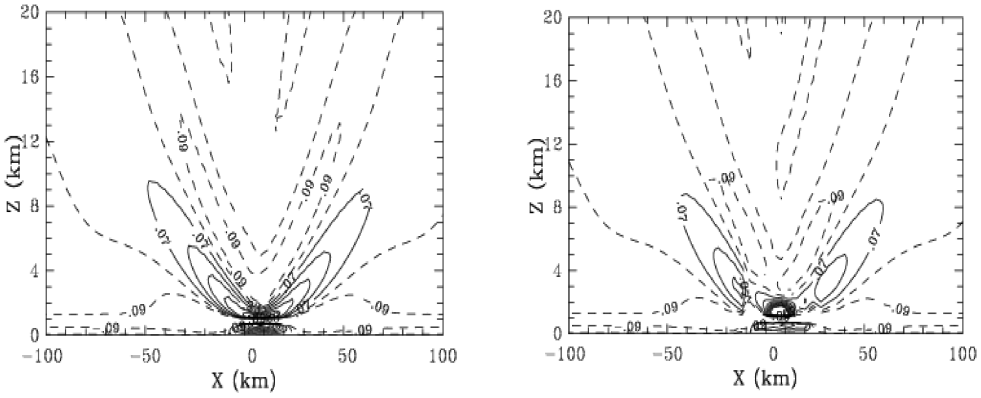

Figure 2.8: Contours for the nonhydrostatic perturbation vertical velocity under constant background profile at $t = 1800$ s (a) $\phi = 5$, (b) $\phi = 10^3$.

(a) **t** = 3 **hrs.** (b) **t** = 3 **hrs.**

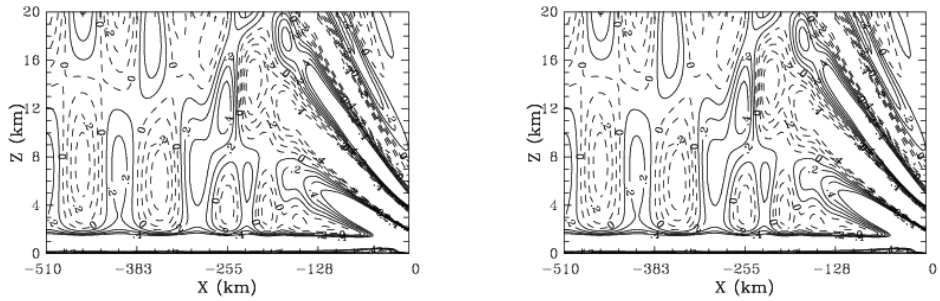

Figure 2.9: Contours for the nonhydrostatic perturbation vertical velocity under constant background profile at $t = 3$ hours (a) $\phi = 5$, (b) $\phi = 10^3$.

(a) **t** = 1800 **seconds** (b) **t** = 1800 **seconds**

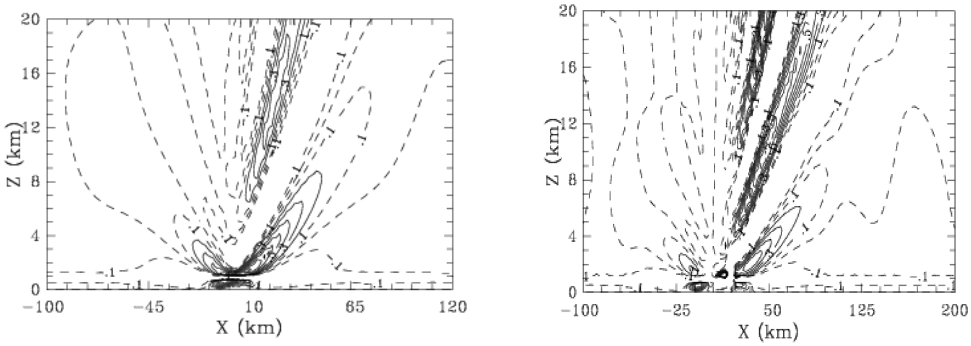

Figure 2.10: Contours for the nonhydrostatic perturbation vertical velocity under shear background profile at $t = 3600$ s (a) $\phi = 5$, (b) $\phi = 10^2$.

(a) **t** = 3 **hrs.** (b) **t** = 3 **hrs.**

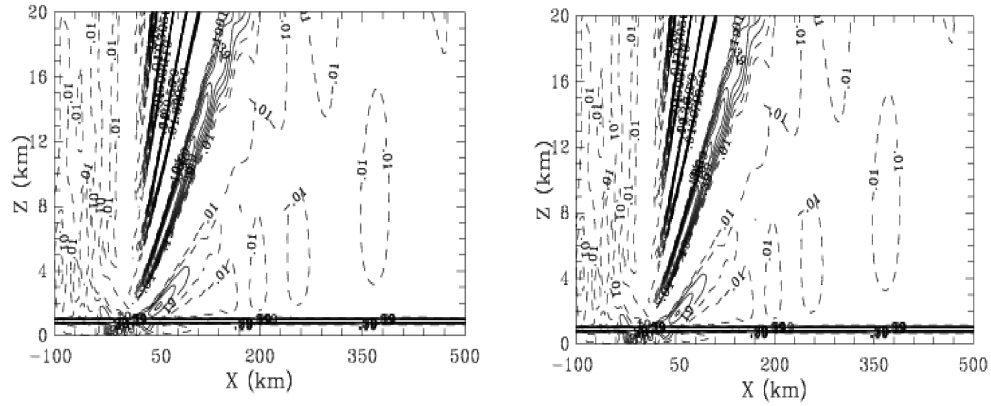

Figure 2.11: Contours for the nonhydrostatic perturbation vertical velocity under shear background profile at $t = 3$ hours (a) $\phi = 5$, (b) $\phi = 10^2$.

The effects of the nonlinearities are found to be negligible as compared to the effects of nonhydrostaticity as shown by the figures (2.8a), (2.9a), (2.10a) and (2.11a). These effects are more relevant in the hydrostatic case [8], where the external forcing is taken to be time independent, bell shaped in x and only within a layer in the $z-$direction. We would also like to make a remark that the splitting of the main moving mode that was observed by Han and Baik in [8] can also be seen here under both constant and the shear backgrounds, in figures (2.8b), (2.9b), (2.10b) and (2.11b). However, for

such a splitting to take place, the strength of the nonlinearities needs to be very high, i.e., the detachment of the moving mode becomes apparent after ϕ is given a value of at least 10^2, which is non-physical. For smaller values of ϕ, the nonhydrostatic effects stay dominant and no detachment is observed. Also, even for large values of the parameter ϕ, the nonhydrostatic effects stay completely unchanged.

Therefore, in summary, considering the observations pointed out above, we can conclude that the hydrostatic assumption wipes out significant amount of dynamics, especially for large values of time, and hence alters the results significantly. The presence of the positive and negative regions along the horizontal direction is observed only for the nonhydrostatic case. Assuming the vertical accelerations to be negligible doesn't depict this particular dynamics at all.

Chapter 3

Linear Instabilities

3.1 Treatment of the forcing function

As mentioned earlier in Chapter 1 that for certain atmospheric processes, it has been shown, for example, in [4], that the presence of moisture in the atmosphere can have a deep effect on the behaviour of the inertia-gravity waves. Also, for the processes like *moist convection*, where we need to allow the feedback of the atmosphere to the latent heating and a well known way to incorporate the effects of the moisture is to assume that the diabatic heating is everywhere proportional to the vertical velocity. Therefore, we will consider that in each layer of the atmosphere $q(w)$ is proportional to $w(t, x, z)$ [4, 13, 14]. We would also like to recall the well known necessary condition that for a diabatic forcing to cause an instability, the forcing must be out of phase with the vertical component w of the velocity vector field [1, 14]. So, we will consider the forcing q to have the form

$$q = q_0 \cos(\alpha) w \quad \text{with} \quad \alpha \neq k\pi/2. \tag{3.1}$$

Taking q proportional to $w(t, x, z)$ in this particular form (3.14) does ignore the 'self-limiting' fact that an air parcel only holds a finite amount of water vapour to condense as it rises above or condensed water to evaporate as it descends. For mathematical simplicity, the domain in this section is considered as $\mathbb{T}^2 = [-\pi, \pi)^2$. However, such a treatment of the domain is inconsistent with the large scale pressure distribution which, rather than being periodic, decreases with altitude.

3.1.1 Reduction of the linearized set of equations

Eliminating the pressure $\pi(t,x,z)$ from $(2.24-2.25)$, we get

$$\frac{\partial}{\partial t}\left(\frac{\partial u}{\partial z}\right) - u_{stat}\left(\frac{\partial^2 w}{\partial z^2}\right) + w\frac{d^2 u_{stat}}{dz^2} = \varepsilon^2\left[\frac{\partial}{\partial t} + u_{stat}\frac{\partial}{\partial x}\right]\frac{\partial w}{\partial x} - \frac{\partial b}{\partial x}. \tag{3.2}$$

Differentiating equation (2.25) with respect to x and using equation (2.27), we get

$$\left(\frac{\partial}{\partial t} + u_{stat}\frac{\partial}{\partial x}\right)\left[\varepsilon^2\frac{\partial^2 w}{\partial x^2} + \frac{\partial^2 w}{\partial z^2}\right] - \frac{\partial w}{\partial x}\frac{d^2 u_{stat}}{dz^2} - \frac{\partial^2 b}{\partial x^2} = 0. \tag{3.3}$$

Using equation (2.26), $b(t,x,z)$ can also be eliminated from the above equation to get the following reduced equation

$$\left(\frac{\partial}{\partial t} + u_{stat}\frac{\partial}{\partial x}\right)^2\left[\varepsilon^2\frac{\partial^2 w}{\partial x^2} + \frac{\partial^2 w}{\partial z^2}\right] - \left(\frac{\partial}{\partial t} + u_{stat}\frac{\partial}{\partial x}\right)\frac{d^2 u_{stat}}{dz^2}\frac{\partial w}{\partial x} = \frac{\partial^2}{\partial x^2}\left[q - w\right]. \tag{3.4}$$

Work presented in subsections $3.1.2-3.1.4$ is a review of the work from [1]. For these subsections, we considering a solution of the form

$$(w(t,x,z), q(t,x,z)) = \mathfrak{R}\left\{(W(z), Q(z))\, e^{ik(x-\sigma t)}\right\}, \tag{3.5}$$

where $\mathfrak{R}$ represents the real part.

3.1.2 Necessary Condition For Instability

The phase velocity with this *ansatz* is given by $\frac{k\sigma_r}{k} = \sigma_r$ and the group velocity will be given by $\frac{d(k\sigma_r)}{dk}$ where σ_r is the real part of σ. Substituting equation (3.5) in equation (3.4), we get the following equation on $w(t,x,z)$

$$\frac{d^2 W}{dz^2} + \left(\frac{1}{(u_{stat}-\sigma)^2} - \frac{1}{(u_{stat}-\sigma)}\frac{d^2 u_{stat}}{dz^2} - \varepsilon^2 k^2\right) W(z) = \frac{Q}{(u_{stat}-\sigma)^2}. \tag{3.6}$$

Defining the following function

$$h(z) = \frac{W(z)}{u_{stat}-\sigma}. \tag{3.7}$$

Now equation (3.6) takes the following form

$$\frac{d}{dz}\left[(u_{stat}-\sigma)^2\frac{dh}{dz}\right]+\left[1-\varepsilon^2k^2(u_{stat}-\sigma)^2\right]h(z)=\frac{Q}{(u_{stat}-\sigma)}. \tag{3.8}$$

Multiplying equation (3.8) by the complex conjugate h^* of h, we get

$$h^*\frac{d}{dz}\left[(u_{stat}-\sigma)^2\frac{dh}{dz}\right]+\left[1-\varepsilon^2k^2(u_{stat}-\sigma)^2\right]|h(z)|^2=-\frac{Qh^*}{(u_{stat}-\sigma)}. \tag{3.9}$$

Integarting equation (3.9) and using integration by parts, we get

$$\int(u_{stat}-\sigma)^2\left|\frac{dh}{dz}\right|^2dz+\int\left[\varepsilon^2k^2(u_{stat}-\sigma)^2-1\right]|h|^2dz=-\int\frac{QW^*}{|u_{stat}-\sigma|^2}dz. \tag{3.10}$$

Taking $\sigma=\sigma_r+i\sigma_i$, the imaginary part of the above equation gives

$$\mathrm{Im}\int(u_{stat}-\sigma)^2\left|\frac{dh}{dz}\right|^2dz+\mathrm{Im}\int\left[\varepsilon^2k^2(u_{stat}-\sigma)^2-1\right]|h|^2dz=\mathrm{Im}\int\frac{QW^*}{|u_{stat}-\sigma|^2}dz, \tag{3.11}$$

which further gives that

$$2\sigma_i\int(u_{stat}-\sigma_r)\left[\left|\frac{dh}{dz}\right|^2+\varepsilon^2k^2|h|^2\right]dz=\mathrm{Im}\int\frac{QW^*}{|u_{stat}-\sigma|^2}dz. \tag{3.12}$$

Using $\sigma=\sigma_r+i\sigma_i$ in equation (3.5) for $w(t,x,z)$, we get

$$w(t,x,z)=W(z)e^{ik(x-\sigma_rt)}e^{k\sigma_it}. \tag{3.13}$$

We consider two different propositions here:

Proposition 1: *For a two-dimensional, non-rotating and boussinesq flow, with zero thermal forcing, for an instability to occur, σ_i must be greater than zero. Also, for the validity of equation (3.12), $(u_{stat}-\sigma_r)$ must change sign somewhere in the domain.*

Let us now consider the following expression for the thermal forcing

$$Q=q_0e^{i\alpha}w. \tag{3.14}$$

Where q_0 and α are real and the phase difference between $w(t,x,z)$ and the thermal forcing is represented by α. Using equation (3.14), the right hand side of equation

(3.12) gives us the following

$$\mathrm{Im}\int \frac{QW^*}{|u_{stat}-\sigma|^2}dz = q_0\int \frac{|W|^2\sin(\alpha)}{|u_{stat}-\sigma|^2}dz \tag{3.15}$$

Proposition 2: *If a diabatic forcing is to cause an amplifying, non-steering instability, then the forcing must be out of phase with the vertical velocity somewhere in the domain [14].*

3.1.3 Condition in terms of the Richardson Number R_i

Using a different substitution given as

$$G(z) = \frac{W(z)}{\sqrt{u_{stat}(z)-\sigma}}. \tag{3.16}$$

Equation (3.6)(with zero forcing) then becomes

$$\frac{d}{dz}\left[(u_{stat}-\sigma)\frac{dG}{dz}\right] + \left[\frac{1}{(u_{stat}-\sigma)} - \frac{1}{4(u_{stat}-\sigma)}\left(\frac{du_{stat}}{dz}\right)^2 - \varepsilon^2k^2(u_{stat}-\sigma) - \frac{1}{2}\frac{d^2u_{stat}}{dz^2}\right]G(z) = 0. \tag{3.17}$$

Which can also be written as

$$\frac{d}{dz}\left[(u_{stat}-\sigma)\frac{dG}{dz}\right] - \left[\frac{\left(\frac{du_{stat}}{dz}\right)^2\left(\frac{1}{4}-\frac{1}{\left(\frac{du_{stat}}{dz}\right)^2}\right)}{(u_{stat}-\sigma)} + \varepsilon^2k^2(u_{stat}-\sigma) + \frac{1}{2}\frac{d^2u_{stat}}{dz^2}\right]G(z) = 0. \tag{3.18}$$

Multiplying equation (3.18) by the complex conjugate $G^*(z)$ of $G(z)$ and integrating, we get

$$\int (u_{stat}-\sigma)^2\left[\left|\frac{dh}{dz}\right|^2 + \varepsilon^2k^2|G|^2\right]dz + \frac{1}{2}\int \frac{d^2u_{stat}}{dz^2}|G|^2\,dz + \int (u_{stat}-\sigma)\left|\frac{G(z)}{(u_{stat}-\sigma)}\right|^2\left(\frac{du_{stat}}{dz}\right)^2\left(\frac{1}{4}-R_i\right)dz = 0. \tag{3.19}$$

Taking $\sigma = \sigma_r + i\sigma_i$, the imagniary part of (3.19) is

$$\sigma_i \left(\int \left[\left| \frac{dG}{dz} \right|^2 + \varepsilon^2 k^2 |G|^2 \right] dz + \int \left| \frac{G(z)}{(u_{stat} - \sigma)} \right|^2 \left(\frac{du_{stat}}{dz} \right)^2 \left(R_i - \frac{1}{4} \right) dz \right) = 0. \tag{3.20}$$

Where $R_i = \frac{N^2}{\left(\frac{du_{stat}}{dz}\right)^2}$ is the *Richardson number. We have that for an instability to occur, we need* $\sigma_i > 0$. *Therefore, equation (3.20) implies that* $R_i < \frac{1}{4}$ *is a necessary condition for an instability in this case.*

3.1.4 Howard's Semi-Circle theorem

The vertical displacement $\eta(t, x, z)$ is defined as

$$w(t, x, z) = \frac{\partial \eta}{\partial t} + u_{stat} \frac{\partial \eta}{\partial x}. \tag{3.21}$$

Recalling (3.5) and taking $\eta(t, x, z) = \xi(z) e^{ik(x - \sigma t)}$, gives

$$\xi(z) = \frac{W(z)}{ik(u_{stat} - \sigma)}. \tag{3.22}$$

Using equation (3.22) in equation (3.6)(with zero forcing), we get

$$\frac{d}{dz} \left[(u_{stat} - \sigma)^2 \frac{d\xi}{dz} \right] + \left[N^2 - \varepsilon^2 k^2 (u_{stat} - \sigma)^2 \right] \xi(z) = 0. \tag{3.23}$$

Multiplying the above equation by the complex conjugate $\xi^*(z)$ of $\xi(z)$, Using integrating by parts, we obtain

$$\int (u_{stat} - \sigma)^2 \left[\left| \frac{d\xi}{dz} \right|^2 + \varepsilon^2 k^2 |\xi|^2 \right] dz - \int |\xi|^2 dz = 0. \tag{3.24}$$

Considering $\sigma = \sigma_r + i\sigma_i$, the real part of equation (3.24) is:

$$\int \left[(u_{stat} - \sigma_r)^2 - \sigma_i^2 \right] \left(\left| \frac{d\xi}{dz} \right|^2 + \varepsilon^2 k^2 |\xi|^2 \right) dz - \int |\xi|^2 dz = 0. \tag{3.25}$$

The imaginary part of equation (3.24) is:

$$2\int \sigma_i(u_{stat}-\sigma_r)\left[\left|\frac{d\xi}{dz}\right|^2+\varepsilon^2k^2|\xi|^2\right]dz=0. \tag{3.26}$$

As, for instability, we need that $(u_{stat}-\sigma_r)$ must change sign between z_1 and z_2, this gives $a<\sigma_r<b$, where $a=u_{stat_{min}}$ and $b=u_{stat_{max}}$. Thus

$$\int (u_{stat}-a)(b-u_{stat})\left[\left|\frac{d\xi}{dz}\right|^2+\varepsilon^2k^2|\xi|^2\right]dz\geq 0. \tag{3.27}$$

Adding equation (3.25) and (3.27), we get

$$\int (\sigma_r^2-2\sigma_r^2u_{stat}-\sigma_i^2+bu_{stat}-ab+au_{stat})\left[\left|\frac{d\xi}{dz}\right|^2+\varepsilon^2k^2|\xi|^2\right]dz-\int|\xi|^2dz\geq 0. \tag{3.28}$$

Multiplying equation (3.26) by $(a+b-2\sigma_r)$, we get

$$\int (u_{stat}-\sigma_r)(a+b-2\sigma_r)\left[\left|\frac{d\xi}{dz}\right|^2+\varepsilon^2k^2|\xi|^2\right]dz=0. \tag{3.29}$$

Subtracting equation (3.29) from (3.28), we get

$$\int (\sigma_r^2+ab-b\sigma_r-a\sigma_r+\sigma_i^2)\left[\left|\frac{d\xi}{dz}\right|^2+\varepsilon^2k^2|\xi|^2\right]dz+\int|\xi|^2dz\leq 0 \tag{3.30}$$

which can further be written as

$$\int\left[\left\{\sigma_r-\left(\frac{a+b}{2}\right)\right\}^2+\sigma_i^2-\left(\frac{a-b}{2}\right)^2\right]\left[\left|\frac{d\xi}{dz}\right|^2+\varepsilon^2k^2|\xi|^2\right]dz+\int|\xi|^2dz\leq 0, \tag{3.31}$$

As the integrand in the second term is positive, we must have that

$$\left\{\sigma_r-\left(\frac{a+b}{2}\right)\right\}^2+\sigma_i^2-\left(\frac{a-b}{2}\right)^2\leq 0, \tag{3.32}$$

or,

$$\left\{\sigma_r-\left(\frac{a+b}{2}\right)\right\}^2+\sigma_i^2\leq\left(\frac{a-b}{2}\right)^2. \tag{3.33}$$

We need $\sigma_i > 0$ for an instability to occur. Therefore, now we state the *Howard's semi-circle theorem* [15]:

Proposition 3: *σ of an unstable normal mode, must lie within the semi-circle that has its center at* $\left(\frac{u_{stat_{min}} + u_{stat_{max}}}{2}, 0\right)$ *and has radius* $\left(\frac{u_{stat_{min}} - u_{stat_{max}}}{2}\right)$.

3.2 Smooth Background

Here we show that for the governing linearized nonhydrostatic equations of mesoscale in the presence of thermal forcing $(2.24) - (2.27)$, a smooth background profile around which the equations are linearized is unstable. To do so, we use the method of continued fraction introduced in [16, 17, 18, 19, 20]. The idea is to use a smooth shear background profile, propose an *ansatz* and then make use of the continued fractions to show the existence of instability. First consider the following definition:

Definition 1. *A stationary solution $\vec{U}_{stat} = (U_{stat}, \theta_{stat})$ of equations $(2.24) - (2.27)$ is said to be linearly unstable, if the spectrum of the linearized operator contains an eigenvalue with a positive real part.*

We would like to point out here that, in the absence of forcing, the stability of a similar sinusoidal background profile ($u_{stat}(y) = \sin y,\ \ y_1 \leq y \leq y_2$) was also discussed by Drazin and Howard [21] and later by Thorpe [22]. Drazin and Howard [21] (using the Taylor-Goldstein equation) and Thorpe [22] (by transforming the Taylor-Goldstein equation to an hyper-geometric equation) used a sinusoidal background to show that the Richardson number criterion is a necessary but not a sufficient condition for instability. Moreover, Drazin and Howard [21] showed that the flow is unstable if $(y_2 - y_1) > \pi$, but stable otherwise although the point of inflection lies within the field of flow. Further, for the same background profile and with the local Richardson number (J) held constant, Drazin and Howard [21] found the three stationary neutral curves (the third was later corrected by Thorpe [22]) and pointed out that for $y_1 = 0, y_2 = \pi$ the flow is known to be stable. Now, consider the following Lemma, showing how to construct such an unstable profile:

Lemma 1. *Considering the thermal forcing $Q = q_0 \cos(\alpha) w$, for fixed q_0 and u_0, the smooth shear background profile $u_{stat}(z) = u_0 \sin(z)$, for a linearized, nonhydrostatic, nonrotating and boussinesq mesoscale flow $(2.24) - (2.27)$, is linearly unstable in the sense of the definition 1 given above.*

Proof. Our goal is to show that for the governing nonhydrostatic equations of Mesoscale in the presence of thermal forcing, the background profile around which the equations are linearized is unstable.
Consider a sinusoidal background shear flow

$$u_{stat}(z) = u_0 \sin(z), \tag{3.34}$$

and make the following *ansatz*:

$$w(t,x,z) = e^{\sigma(k)t} \sin(kx) \sum_{p=-\infty}^{+\infty} c_p \cos(pz) \tag{3.35}$$

Here the parameter $k \in \mathbb{Z}$ and we are trying to find $k, \sigma(k), (c_p)_p$ such that the $\sigma(k) > 0$ and $w(t,x,z)$ solves the reduced equation (3.4). Substituting equations $(3.34) - (3.35)$ in equation (3.4), we get

$$\begin{aligned}
\sin(kx) \quad & \sum_{p=-\infty}^{+\infty} \left[\left(\sigma^2 - \frac{k^2u_0^2}{2} \right) \left[\varepsilon^2 k^2 + p^2 \right] + \frac{k^2u_0^2}{2} + k^2 - \gamma k^2 \right] c_p \cos(pz) \\
+ \quad & \sin(kx) \sum_{p=-\infty}^{+\infty} \left(\frac{k^2u_0^2}{4} \left[\varepsilon^2 k^2 + (p-2)^2 \right] - \frac{k^2u_0^2}{4} \right) c_{p-2} \cos(pz) \\
+ \quad & \sin(kx) \sum_{p=-\infty}^{+\infty} \left(\frac{k^2u_0^2}{4} \left[\varepsilon^2 k^2 + (p+2)^2 \right] - \frac{k^2u_0^2}{4} \right) c_{p+2} \cos(pz) \\
+ \quad & \cos(kx) \sum_{p=-\infty}^{+\infty} \left(u_0 \sigma k \left[\varepsilon^2 k^2 + (p+1)^2 \right] - \frac{u_0 \sigma k}{2} \right) c_{p+1} \sin(pz) \\
- \quad & \cos(kx) \sum_{p=-\infty}^{+\infty} \left(u_0 \sigma k \left[\varepsilon^2 k^2 + (p-1)^2 \right] - \frac{u_0 \sigma k}{2} \right) c_{p-1} \sin(pz) = 0,
\end{aligned} \tag{3.36}$$

with $\gamma = q_0 \cos(\alpha)$. Defining

$$a_{\sigma,p} = \left(\sigma^2 - \frac{k^2u_0^2}{2} \right) \left[\varepsilon^2 k^2 + p^2 \right] + \frac{k^2u_0^2}{2} + k^2 - \gamma k^2, \tag{3.37a}$$

$$b_p = \frac{k^2u_0^2}{4} \left[\varepsilon^2 k^2 + p^2 - 1 \right], \tag{3.37b}$$

$$d_p = (u_0 \sigma k) \left[\varepsilon^2 k^2 + p^2 - \frac{1}{2} \right], \tag{3.37c}$$

then equation (3.36) gives us the following recurrence identities

$$a_{\sigma,p}c_p + b_{p-2}c_{p-2} = -b_{p+2}c_{p+2}, \tag{3.38a}$$

$$d_{p-1}c_{p-1} = d_{p+1}c_{p+1}. \tag{3.38b}$$

Dividing equation (3.38a) by $c_p b_p$ and setting

$$\rho_p(\sigma) = \frac{c_p b_p}{c_{p-2}b_{p-2}} \qquad \text{for} \qquad p > 0, \tag{3.39a}$$

$$\tilde{\rho}_p(\sigma) = \frac{c_{p-2}b_{p-2}}{c_p b_p} \qquad \text{for} \qquad p \leq 0, \tag{3.39b}$$

and

$$\alpha_p(\sigma) = \frac{a_{\sigma,p}}{b_p}. \tag{3.39c}$$

Using equation (3.39a), equation (3.38a) transforms into the following

$$\alpha_p + \frac{1}{\rho_p} = -\rho_{p+2}, \tag{3.40}$$

which further becomes

$$\rho_p(\sigma) = \frac{-1}{\alpha_p(\sigma) - \frac{1}{\alpha_{p+2}(\sigma) - \frac{1}{\alpha_{p+4}(\sigma) - \frac{1}{\alpha_{p+6}(\sigma) - \cdots}}}}. \tag{3.41}$$

Also, using equation (3.39b), equation (3.38a) transforms into the following

$$\alpha_p + \tilde{\rho}_p = -\frac{1}{\tilde{\rho}_{p+2}}. \tag{3.42}$$

Equation (3.42) with $p = -2$ becomes

$$\tilde{\rho}_0(\sigma) = \frac{-1}{\alpha_{-2}(\sigma) + \tilde{\rho}_{-2}}. \tag{3.43}$$

Using equations $(3.39a - 3.39b)$, equation (3.38a) gives

$$-\rho_{p+2} = \alpha_p + \tilde{\rho}_p. \tag{3.44}$$

which for $p = 0$ becomes

$$-\rho_2 = \alpha_0 + \tilde{\rho}_0 = \frac{-1}{\alpha_{-2} + \tilde{\rho_{-2}}}, \tag{3.45}$$

Note that as $p \to \infty$

$$\rho_\infty = \tilde{\rho}_\infty = -\frac{\alpha_\infty}{2} + \sqrt{\left(\frac{\alpha_\infty}{2}\right)^2 - 1},$$

and as $\alpha_{-p} = \alpha_p$, one can easily check that $\rho_2 = \tilde{\rho}_0$. Equation (3.45) then gives

$$\frac{\alpha_0}{2} = \cfrac{1}{\alpha_2(\sigma) - \cfrac{1}{\alpha_4(\sigma) - \cfrac{1}{\alpha_6(\sigma) - \cfrac{1}{\alpha_8(\sigma) - \ldots}}}} \equiv F(\sigma) \tag{3.46}$$

Our goal is to find a real, positive solution σ of equation (3.46). The right hand side of equation (3.46) is a continued fraction. To determine the convergence of this continued fraction, we consider the following result by Śleszyński-Pringsheim [23]:

Lemma 2. *Given two sequences of real numbers* (a_n) *and* (b_n) *such that* $|b_n| \geq |a_n| + 1$ *for all* n*, then the continued fraction*

$$\cfrac{a_1}{b_1 + \cfrac{a_2}{b_2 + \cfrac{a_3}{b_3 + \ldots}}}$$

converges absolutely to a number f *satisfying* $0 < |f| < 1$*.*

Now considering the right hand side of equation (3.46), the sufficient condition for the convergence of $F(\sigma)$ becomes

$$\alpha_p(\sigma) \geq 2.$$

Using the fact that (α_p) is non-increasing, then $\alpha_\infty(\sigma) := \lim_{p \to \infty}(\sigma)$ is the smallest $\alpha_p(\sigma)$, the sufficient condition thus becomes

$$\alpha_\infty(\sigma) \geq 2.$$

Using equations (3.37a-3.37b) and equation (3.39c), we can easily find that

$$\frac{\left(\sigma^2 - \frac{k^2u_0^2}{2}\right)}{\frac{k^2u_0^2}{4}} \geq 2,$$

which reduces to the following condition for the convergence of $F(\sigma)$

$$|\sigma| \geq ku_0. \tag{3.47}$$

Notice that

$$c_{2p} = \left(\frac{c_0 b_0}{b_{2p}}\right) \rho_2\rho_4\rho_6 \cdots \rho_{2p}. \tag{3.48}$$

and

$$c_{-2p} = \left(\frac{c_0 b_0}{b_{2p}}\right) \tilde{\rho}_0\tilde{\rho}_{-2}\tilde{\rho}_{-4} \cdots \tilde{\rho}_{-2(p-1)}. \tag{3.49}$$

Choosing $c_{-1} = 0$, we can use the recurrence relation (3.38b) to show that c_{2p+1} is zero. Also, c_{2p} and c_{-2p} satisfy equations (3.40) and (3.42), respectively. Further, as ρ_p is bounded for every p (guaranteed by Lemma 2), using equation (3.48) and (3.49), we can write that $c_{2p}, c_{-2p} \to 0$ as $p \to \infty$. Having found ρ_2 using equation (3.46), we can then find ρ_p for all values of p using equations (3.40) $-$ (3.42). Further, c_{2p} and c_{-2p} for all values of p can be found using equations (3.48) $-$ (3.49) and therefore the recurrence relation (3.38a) is satisfied.
To show that if $c_p \to 0$, then $p^2c_p \to 0$, we use the notation $A = \left(\sigma^2 - \frac{k^2u_0^2}{2}\right) > 0, B = \left(\sigma^2 - \frac{k^2u_0^2}{2}\right)(\varepsilon^2k^2) + \frac{k^2u_0^2}{2} + k^2 - \gamma k^2, \tilde{A} = \left(\frac{k^2u_0^2}{4}\right) > 0$ and $\tilde{B} = \frac{k^2u_0^2}{4}[\varepsilon^2k^2 - 1]$. One can then write equation (3.38a) as

$$(Ap^2 + B)c_p + \tilde{A}(p-2)^2c_{p-2} + \tilde{B}c_{p-2} = -\tilde{A}(p+2)^2c_{p+2} - \tilde{B}c_{p+2} \tag{3.50}$$

Assuming $\lim_{p\to\infty} p^2c_p = l$, equation (3.50) implies that $l = \lim_{p\to\infty} p^2c_p = 0$. Further, using equation (3.48) or (3.49) and the fact that ρ_p converges to a value between 0 and 1 for all p, we can show that p^2c_p does possess a limit.
Given that the condition in equation (3.47) is satisfied, Lemma 2 guarantees that the

right hand side of equation (3.46) satisfies that

$$0 < F(\sigma) < 1 \tag{3.51}$$

Now fixing $u_0 = 1, k = 2, \gamma = 5.2$ and $\varepsilon = 1$, a straightforward calculation shows that

$$\alpha_0(\sigma)|_{\sigma=2.1} = -1.72, \qquad \text{and} \qquad \alpha_0(\sigma)|_{\sigma=2.7} = 2.12. \tag{3.52}$$

Using equation (3.52), equation (3.51) implies that

$$0.86 < F(\sigma) - \frac{\alpha_0(\sigma)}{2}\bigg|_{\sigma=2.1} < 1.86$$

and

$$-1.06 < F(\sigma) - \frac{\alpha_0(\sigma)}{2}\bigg|_{\sigma=2.7} < -0.06$$

Therefore, equation (3.46) must have a solution σ. Moreover, for $2.1 \leq \sigma \leq 2.7$. □

The following plot shows $F(\sigma)$ truncated at six terms and $F(\sigma)$ truncated at 1000 terms.

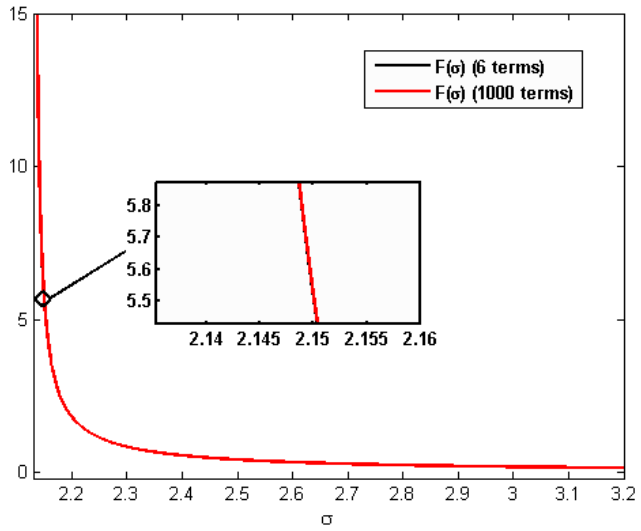

Figure 3.1: Plots for $F(\sigma)$ with different truncations. Values of the parameters used are $u_0 = 1, k = 2, \gamma = 5.2, \varepsilon = 1$.

Consider the following plots now:

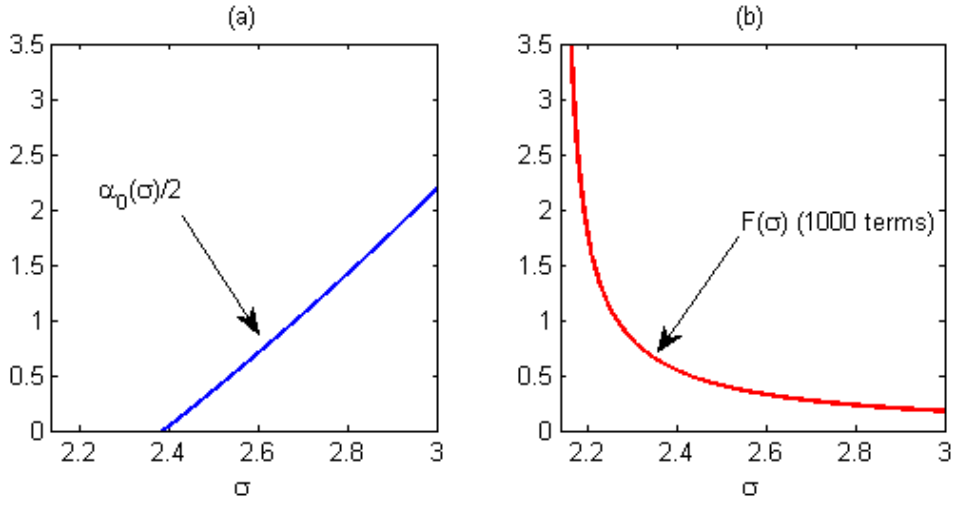

Figure 3.2: Plots of the left and right hand side of equation (3.46): **(a)** $\frac{\alpha_0(\sigma)}{2}$, **(b)** $F(\sigma)$. Values of the parameters used are $u_0 = 1, k = 2, \gamma = 5.2, \varepsilon = 1$.

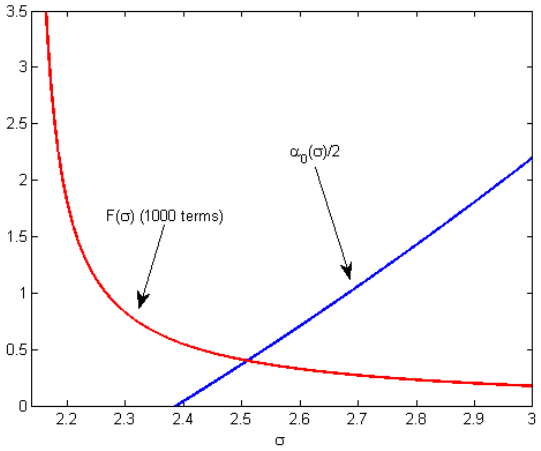

Figure 3.3: Plots of $\frac{\alpha_0(\sigma)}{2}$ and $F(\sigma)$. Values of the parameters used are $u_0 = 1, k = 2, \gamma = 5.2, \varepsilon = 1$.

Figure (3) shows that equation (3.46) has a solution at $\sigma \approx 2.46$. This value clearly belongs to the region of convergence of $F(\sigma)$.

Remark: Here, we would like to point out that in the absence of thermal forcing, i.e., $q(t, x, z) = 0$, the solution of equation (3.46) moves to the region where the condition (3.47) for the convergence of the continued fraction in (3.46) is not satisfied. In order to get the instability, one then has to consider the Brunt-Väisälä frequency $N \gg 1$,

which is non-physical.

3.3 Discontinuous Background

In this section, we show the instability for a background that has a jump discontinuity somewhere in the domain. The idea [24] here will be to consider a wave type solution, make use of a specific type of boundary conditions and then use the dispersion relation by applying the *matching conditions* at the point of discontinuity of the background profile to show the existence of instability. The thermal forcing will be considered zero in this section. The necessary condition is derived for the general set of equations but the case of zero forcing is also discussed. The domain is considered to be infinite in the $x-$direction and bounded by two rigid layers in the vertical located at $z = z_1$ and $z = z_2$ for some $z_1, z_2 \in \mathbb{R}$. The boundary conditions are considered as $w(t, x, z) = 0$ at $z = z_1, z_2$. The forcing will be considered zero in this case. Consider the following Lemma

Lemma 3. *Consider the following background profile*

$$u_{stat}(z) = \begin{cases} +1, & z > z_0 \\ -1, & z < z_0 \end{cases} \tag{3.53}$$

For a linearized, nonhydrostatic, non-rotating and boussinesq flow with zero thermal forcing, such a background profile is linearly unstable.

Proof. Now the idea is to solve for $W(z)$ in two different regions. Namely, the region $z < z_0$ and the region $z > z_0$. In either of the above defined regions, $u_{stat}(z)$ is continuous and thus $W(z)$ can be computed easily. For doing so, we need to introduce the *matching conditions* at the interface $z = z_0$. Firstly, we consider that $W(z)$ is continuous across the interface, i.e.

$$\lim_{\epsilon \to 0} \left[W(z)|_{z_0+\epsilon} - W(z)|_{z_0-\epsilon} \right] = 0. \tag{3.54}$$

The expression for vertical displacement of the fluid is given in equation (3.22). For the continuiuty of the vertical displacement of the fluid across the interface $z = z_0$,

we get the following condition

$$\lim_{\epsilon\to 0}\left\{\left[\frac{W(z)}{u_{stat}-\sigma}\right]\Big|_{z_0+\epsilon} - \left[\frac{W(z)}{u_{stat}-\sigma}\right]\Big|_{z_0-\epsilon}\right\} = 0, \tag{3.55}$$

Differentiating equation (2.24) with respect to x, we get

$$\left(\frac{\partial}{\partial t} + u_{stat}\frac{\partial}{\partial x}\right)\frac{\partial u}{\partial x} + \frac{\partial w}{\partial x}\frac{du_{stat}}{dz} = -\frac{\partial^2\pi}{\partial x^2}, \tag{3.56}$$

Now using the continuiuty equation (2.27), the above equation becomes

$$-\left(\frac{\partial}{\partial t} + u_{stat}\frac{\partial}{\partial x}\right)\frac{\partial w}{\partial z} + \frac{\partial w}{\partial x}\frac{du_{stat}}{dz} = -\frac{\partial^2\pi}{\partial x^2}, \tag{3.57}$$

Now using equation (3.5) for $w(t,x,z)$ and $\pi(t,x,z)$, i.e.

$$(w,\pi)(t,x,z) = (W,\Pi)(z)e^{ik(x-\sigma t)}. \tag{3.58}$$

This reduces equation (3.57) to the following

$$-(ik)(u_{stat}-\sigma)\frac{dW}{dz} + (ik)W(z)\frac{du_{stat}}{dz} = -(ik)^2\Pi, \tag{3.59}$$

which simplifies to

$$\frac{1}{(ik)}\left[(u_{stat}-\sigma)\frac{dW}{dz} - W(z)\frac{du_{stat}}{dz}\right] = \Pi, \tag{3.60}$$

Therefore, for the continuity of pressure across the interface, we get

$$\lim_{\epsilon\to 0}\left\{\left[(u_{stat}-\sigma)\frac{dW}{dz} - W(z)\frac{du_{stat}}{dz}\right]\Big|_{z_0+\epsilon} - \left[(u_{stat}-\sigma)\frac{dW}{dz} - W(z)\frac{du_{stat}}{dz}\right]\Big|_{z_0-\epsilon}\right\} = 0. \tag{3.61}$$

Using the background profile (3.53), equation (3.6) (with zero forcing) can now be written as

$$\begin{cases} \frac{d^2W}{dz^2} - \left(\varepsilon^2k^2 - \frac{N^2}{(1-\sigma)^2}\right)W(z) = 0, & z > z_0 \\ \frac{d^2W}{dz^2} - \left(\varepsilon^2k^2 - \frac{N^2}{(1+\sigma)^2}\right)W(z) = 0. & z < z_0 \end{cases} \tag{3.62}$$

Equation (3.62) has the following solution

$$W(z) = \begin{cases} c_2 e^{-\beta_1 (z - z_0)}, & z > z_0 \\ c_1 e^{\beta_2 (z - z_0)}, & z < z_0 \end{cases} \tag{3.63}$$

where

$$\beta_1 = \left(\varepsilon^2 k^2 - \frac{N^2}{(1-\sigma)^2} \right)^{\frac{1}{2}} \tag{3.64a}$$

$$\beta_2 = \left(\varepsilon^2 k^2 - \frac{N^2}{(1+\sigma)^2} \right)^{\frac{1}{2}}. \tag{3.64b}$$

Therefore,

$$w(t,x,z) = \begin{cases} c_2 e^{-\beta_1 (z - z_0) + ik(x - \sigma t)}, & z > z_0 \\ c_1 e^{\beta_2 (z - z_0) + ik(x - \sigma t)}, & z < z_0 \end{cases} \tag{3.65}$$

Using the matching condition (3.55) and (3.61), we get

$$c_1(\sigma - 1) = c_2(\sigma + 1), \tag{3.66}$$

$$\beta_2 c_1(-1 - \sigma) = -\beta_1 c_2(1 - \sigma). \tag{3.67}$$

Using the values of β_1 and β_2 and eliminating c_1 and c_2 from the above two equations, we get

$$\sigma^3 + \left(1 - \frac{2N^2}{4\varepsilon^2 k^2} \right) \sigma = 0. \tag{3.68}$$

This polynomial has one real root $\sigma = 0$ and the other two are complex conjugates. □

3.4 Linear Shear (up to a height H)

Again the forcing will be considered zero in this section. We have the following theorem:

Lemma 4. *Considering*

$$u_{stat}(z) = \begin{cases} +H, & z > H \\ z, & -H < z < H \\ -H, & z < -H \end{cases} \tag{3.69}$$

For a linearized, both hydrostatic and nonhydrostatic, non-rotating and boussinesq flow with zero thermal forcing, such a background profile is linearly unstable.

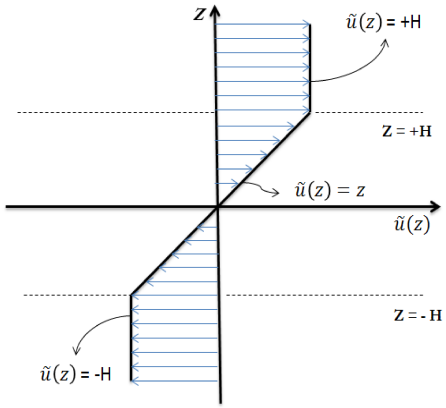

Figure 3.4: Background profile with linear shear.

Proof. The above background profile was also considered by Goldstein [25] to show the that the *Rayleigh's inflection point theorem* is not a sufficient condition for instability. Along with that, we will consider zero thermal forcing and the background potential temperature to be constant. With these considerations, equation (3.4) (with zero forcing) takes the following form

$$\left(\frac{\partial}{\partial t}+u_{stat}\frac{\partial}{\partial x}\right)^2\left[\varepsilon^2\frac{\partial^2 w}{\partial x^2}+\frac{\partial^2 w}{\partial z^2}\right]-\left(\frac{\partial}{\partial t}+u_{stat}\frac{\partial}{\partial x}\right)\frac{d^2u_{stat}}{dz^2}\frac{\partial w}{\partial x}=0. \tag{3.70}$$

with $u_{stat}(z)$ given in (3.69). Again considering a wave type solution, i.e.

$$w(t,x,z)=W(z)e^{ik(x-\sigma t)}. \tag{3.71}$$

Using equation (3.71) in (3.70), we get the following equation

$$\frac{d^2W}{dz^2}-\left(\varepsilon^2k^2\right)W(z)=0. \tag{3.72}$$

Taking $\beta=\varepsilon|k|$ and considering the type of background we have, the above equation

has the following solution

$$W(z) = \begin{cases} c_1 e^{-\beta z} + c_2 e^{\beta z}, & z > H \\ c_4 e^{-\beta z} + c_3 e^{\beta z}, & -H < z < H \\ c_5 e^{-\beta z} + c_6 e^{\beta z}, & z < -H \end{cases} \tag{3.73}$$

Using the upper and lower radiation boundary conditions, the above solution takes the following form

$$W(z) = \begin{cases} c_1 e^{-\beta z}, & z > H \\ c_3 e^{\beta z} + c_4 e^{-\beta z}, & -H < z < H \\ c_6 e^{\beta z}, & z < -H \end{cases} \tag{3.74}$$

To find the unknown constants c_1, c_3, c_4 and c_6, we will use the continuity of both the vertical displacement and the continuity of the pressure at the interfaces $z = -H$ and $z = H$. First, at the interface $z = -H$, the continuity of the vertical displacement and the continuity of the pressure, respectively, are given as

$$\lim_{\epsilon \to 0} \left\{ \left[\frac{W(z)}{u_{stat} - \sigma} \right] \Big|_{-H+\epsilon} - \left[\frac{W(z)}{u_{stat} - \sigma} \right] \Big|_{-H-\epsilon} \right\} = 0, \tag{3.75}$$

$$\lim_{\epsilon \to 0} \left\{ \left[(u_{stat} - \sigma) \frac{dW}{dz} - W(z) \frac{du_{stat}}{dz} \right] \Big|_{-H+\epsilon} - \left[(u_{stat} - \sigma) \frac{dW}{dz} - W(z) \frac{du_{stat}}{dz} \right] \Big|_{-H-\epsilon} \right\} = 0. \tag{3.76}$$

Similarly, for the interface at $z = H$, we have

$$\lim_{\epsilon \to 0} \left\{ \left[\frac{W(z)}{u_{stat} - \sigma} \right] \Big|_{H+\epsilon} - \left[\frac{W(z)}{u_{stat} - \sigma} \right] \Big|_{H-\epsilon} \right\} = 0, \tag{3.77}$$

$$\lim_{\epsilon \to 0} \left\{ \left[(u_{stat} - \sigma) \frac{dW}{dz} - W(z) \frac{du_{stat}}{dz} \right] \Big|_{H+\epsilon} - \left[(u_{stat} - \sigma) \frac{dW}{dz} - W(z) \frac{du_{stat}}{dz} \right] \Big|_{H-\epsilon} \right\} = 0. \tag{3.78}$$

Using equations (3.75) and (3.76), we get the following, respectively

$$c_6 = \left[c_3 e^{-\beta H} + c_4 e^{\beta H} \right] e^{\beta H} \tag{3.79}$$

$$c_6 = \frac{1}{\beta(H + \sigma)} \left[(\beta(\sigma + H) + 1)\, c_3 e^{-\beta H} - (\beta(\sigma + H) - 1)\, c_4 e^{\beta H} \right] e^{\beta H} \tag{3.80}$$

Similarly, (3.77) and (3.78) gives us the following, respectively

$$c_1 = \left[c_3 e^{\beta H} + c_4 e^{-\beta H}\right] e^{\beta H} \tag{3.81}$$

$$c_1 = \frac{1}{\beta(H-\sigma)} \left[(1-\beta(H-\sigma))\, c_3 e^{\beta} - (1+\beta(H-\sigma))\, c_4 e^{-\beta}\right] e^{\beta} \tag{3.82}$$

Equating equation (3.80) with (3.79) and equation (3.82) with (3.81), we, respectively, get the following equations

$$\left(\frac{\beta(\sigma+H)+1}{\beta(H+\sigma)} - 1\right) e^{-\beta H} c_3 - \left(\frac{\beta(\sigma+H)-1}{\beta(H+\sigma)} + 1\right) e^{\beta H} c_4 = 0, \tag{3.83}$$

$$\left(\frac{\beta(\sigma-H)+1}{\beta(H-\sigma)} - 1\right) e^{\beta H} c_3 - \left(\frac{\beta(\sigma-H)-1}{\beta(H-\sigma)} + 1\right) e^{-\beta H} c_4 = 0. \tag{3.84}$$

The above two equations can also be written as

$$\underbrace{\begin{bmatrix} \left(\frac{\beta(\sigma+H)+1}{\beta(H+\sigma)} - 1\right) e^{-\beta H} & -\left(\frac{\beta(\sigma+H)-1}{\beta(H+\sigma)} + 1\right) e^{\beta H} \\ \left(\frac{\beta(\sigma-H)+1}{\beta(H-\sigma)} - 1\right) e^{\beta H} & -\left(\frac{\beta(\sigma-H)-1}{\beta(H-\sigma)} + 1\right) e^{-\beta H} \end{bmatrix}}_{\mathbf{A}} \underbrace{\begin{bmatrix} c_3 \\ c_4 \end{bmatrix}}_{\mathbf{C}} = \underbrace{\begin{bmatrix} 0 \\ 0 \end{bmatrix}}_{\mathbf{0}} \tag{3.85}$$

For the non-trivial solution of $\mathbf{C}$, the determinent of the matrix $\mathbf{A}$ must be zero, which gives

$$\begin{aligned} &\left[\left(\frac{\beta(\sigma+H)+1}{\beta(H+\sigma)} - 1\right) e^{-\beta H}\right] \left[-\left(\frac{\beta(\sigma-H)-1}{\beta(H-\sigma)} + 1\right) e^{-\beta H}\right] \\ &= \left[-\left(\frac{\beta(\sigma+H)-1}{\beta(H+\sigma)} + 1\right) e^{\beta H}\right] \left[\left(\frac{\beta(\sigma-H)+1}{\beta(H-\sigma)} - 1\right) e^{\beta H}\right] \end{aligned} \tag{3.86}$$

$$e^{-4\beta H} = -\left[2\beta(H+\sigma) - 1\right] \left[2\beta(\sigma-H) + 1\right] \tag{3.87}$$

Rearranging the above and using the expression for β, we get the following

$$\sigma^2 = \left[\frac{e^{-4\varepsilon|k|H} - (1-2\varepsilon|k|H)^2}{4\varepsilon^2 k^2}\right]. \tag{3.88}$$

The numerator $\left[e^{-4\varepsilon|k|H} - (1-2\varepsilon|k|H)^2\right]$ is greater than zero for small $k > 0$, which

corresponds to long-wavelength unstable modes. Therefore

$$\sigma = \pm i \left[\frac{-e^{-4\varepsilon|k|H} + (1 - 2\varepsilon|k|H)^2}{4\varepsilon^2 k^2} \right]^{\frac{1}{2}}. \tag{3.89}$$

Expanding $e^{-4\varepsilon kH} = 1 - (4\varepsilon kH) + (4\varepsilon kH)^2 - (4\varepsilon kH)^3 + \cdots$, equation (3.89) becomes

$$\sigma = \pm i \left[\frac{\left(1 - (4\varepsilon kH) + \frac{1}{2!}(4\varepsilon kH)^2 - \frac{1}{3!}(4\varepsilon kH)^3 + \cdots\right) - (1 - 2\varepsilon kH)^2}{4\left(\varepsilon k\right)^2} \right]^{\frac{1}{2}}, \tag{3.90}$$

which simplifies to

$$\sigma = \pm i \left[H^2 - \frac{4^2}{3!}(\varepsilon kH) + \frac{4^3}{4!}(\varepsilon kH)^2 + \cdots \right]^{\frac{1}{2}}, \tag{3.91}$$

Taking $\lim_{\varepsilon \to 0}$ of the above for the hydrostatic case (which, as pointed out earlier in Chapter 2, is also comparable to taking the long-wavelength limit of the dynamics of the flow), gives

$$\sigma = \pm\, iH. \tag{3.92}$$

Therefore, we also have instability for the hydrostatic case for both short and long-wavelength waves. □

3.5 Shear Background (linear in z)

In this section, we point out a linear instability that we noticed for the case of a shear background profile that increases linearly to infinity with height, i.e., with $u_{stat}(z) = -\alpha z$. Considering the hydrostatic assumption and considering the above mentioned background profile, equation (3.4), in the Laplace ($t \to s$) and Fourier ($x \to k$) spaces can be written as (with $q(w) = \gamma w$)

$$\frac{\partial^2 \hat{w}}{\partial z^2} + \phi^2 \lambda^2 \hat{w} = 0, \tag{3.93}$$

with

$$\lambda^2 = \frac{(ik)^2}{(s + iku_{stat})^2}, \qquad \phi^2 = 1 - \gamma. \tag{3.94}$$

Using the upper radiation boundary condition, and assuming a mountain type profile at the ground, i.e.,

$$\hat{w}(t,x,0) = \frac{h_0 a^2}{a^2+x^2},$$

the solution to the differential equation (3.93) can be written as

$$\hat{w}(s,k,z) = a h_0 e^{-a|k|} \left[s + iku_{stat}(0)\right]^{-1/2+i\beta} \left[s + iku_{stat}(z)\right]^{1/2-i\beta}, \tag{3.95}$$

where $\beta = \sqrt{\frac{\phi^2}{\alpha^2} - \frac{1}{4}}$. Following a similar procedure laid out in [6], we can write the solution in the physical space as

$$w(t,x,z) = \frac{C}{2a}\Re(I_1 + I_2), \tag{3.96}$$

where

$$\begin{aligned} I_1 &= -\frac{\pi}{t\cos(\pi\beta)}\bar{S}_h^{-3/2+i\beta}(\bar{S}_h+\bar{m})^{1/2-i\beta} \\ &\quad -\frac{\pi}{t\cos[\pi(i-\beta)]}\bar{S}_h^{-1/2+i\beta}(\bar{S}_h+\bar{m})^{-1/2-i\beta}, \end{aligned} \tag{3.97}$$

$$\begin{aligned} I_2 &= -\frac{\pi}{t\cos(\pi\beta)}S_h^{-3/2+i\beta}(S_h+m)^{1/2-i\beta} \\ &\quad -\frac{\pi}{t\cos[\pi(i-\beta)]}S_h^{-1/2+i\beta}(S_h+m)^{-1/2-i\beta}, \end{aligned} \tag{3.98}$$

and

$$\begin{aligned} S_h &= a - i[x - u_{stat}(0)t] \qquad m = it\left[u_{stat}(z) - u_{stat}(0)\right], \\ \bar{S}_h &= a + i[x - u_{stat}(0)t] \qquad \bar{m} = it\left[u_{stat}(0) - u_{stat}(z)\right], \end{aligned} \tag{3.99}$$

and $C = \dfrac{a^2 h_0}{\Gamma(1/2 - i\beta)\Gamma(-1/2 + i\beta)}$. Now consider the following plot.

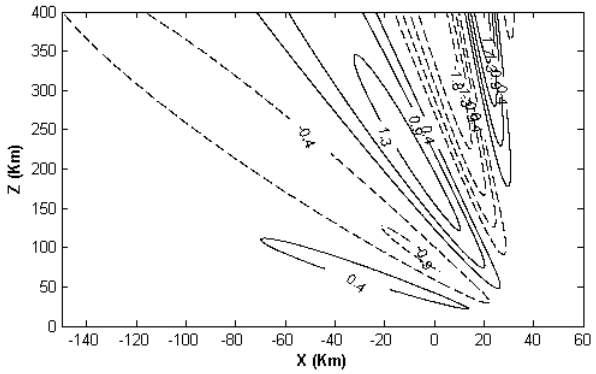

Figure 3.5: Contours for the $w(t, x, z)$ at $t = 1$ hr. Values of the parameters used are given by: $a = 10$ Km, $h_0 = 1$ Km, $\gamma = 0.5$ and $\alpha = 0.0025$ s^{-1}. The contours are rescaled by 10^{-10}.

It has been observed that the solution stays finite as long as the parameter γ stays less than 1. As soon as γ goes bigger than 1, the instability sets in and the solution goes to infinity.

Chapter 4

The Nonlinear Problem and Instabilities

In this chapter we, first, investigate local well-posedness of the governing set of equations and then further show that the established linear unstable mode is also nonlinearly unstable. To show the well-posedness, we use the method outlined in [26]. For mathematical simplicity, we will consider the temperature to be constant T_0. With this, the governing set of nonlinear equations can be written as

$$\frac{\partial u}{\partial t} + u\frac{\partial u}{\partial x} + w\frac{\partial u}{\partial z} = -\frac{1}{\rho_0}\frac{\partial p}{\partial x}, \qquad (x,z) \in \Omega \tag{4.1}$$

$$\frac{\partial w}{\partial t} + u\frac{\partial w}{\partial x} + w\frac{\partial w}{\partial z} = -\frac{1}{\rho_0}\frac{\partial p}{\partial z} - g\frac{\rho}{\rho_0}, \tag{4.2}$$

$$\frac{\partial \theta}{\partial t} + u\frac{\partial \theta}{\partial x} + w\frac{\partial \theta}{\partial z} = \frac{\theta}{c_p T_0}q, \tag{4.3}$$

$$\frac{\partial u}{\partial x} + \frac{\partial w}{\partial z} = 0. \tag{4.4}$$

Letting $m > 2$ and denoting $V^m = \{U \in H^m(\mathbb{T}^2) : \operatorname{div} U = 0\}$, we state the first result regarding the well-posedness:

Theorem 1. *For any $(U_0, \theta_0) \in V^m(\mathbb{T}^2) \times H^m(\mathbb{T}^2)$, there exists a positive time $T = T\left(\|U_0\|_{H^m}, \|\theta_0\|_{H^m}\right)$ such that the system of equations $(4.1) - (4.4)$ has a unique solution $(U, \theta) \in C\left([0,T]; V^m \times H^m\right)$.*

4.1 Proof of Theorem 1

Proof. The method used in this section is classical and is based on the regularization of our equations $(4.1)-(4.4)$ using a mollifier. Then pass to the limit.
Using equation (3.1) and regularizing the governing equations $(4.1)-(4.4)$, we write (with normalized constants)

$$\begin{cases} \frac{\partial U^\epsilon}{\partial t} + \mathcal{J}_\epsilon\left\{\left(\mathcal{J}_\epsilon U^\epsilon\right).\nabla\left(\mathcal{J}_\epsilon U^\epsilon\right)\right\} = -\nabla p^\epsilon + \theta^\epsilon \hat{e}_2, \qquad (x,z)\in\Omega \\ \\ \frac{\partial \theta^\epsilon}{\partial t} + \mathcal{J}_\epsilon\left\{\left(\mathcal{J}_\epsilon U^\epsilon\right).\nabla\left(\mathcal{J}_\epsilon \theta^\epsilon\right)\right\} = \mathcal{J}_\epsilon\{\left(\mathcal{J}_\epsilon \theta^\epsilon\right).\left(\mathcal{J}_\epsilon w^\epsilon\right)\}, \\ \\ \operatorname{div}\left(v^\epsilon\right) = 0. \end{cases} \tag{4.5}$$

Where $U^\epsilon = (u^\epsilon, w^\epsilon)$ and $\hat{e}_2 = (0,1)$ is the unit vector along the $z-$axis. The above set of equations (4.5) is inspired by the general set of mesoscale equations (2.1)-(2.5) but is not exactly the same as the one in (2.1)-(2.5). The unphysical treatment of the temperature T and the replacement of the density ρ/ρ_0 by the potential temperature θ/θ_0 in equation (4.5) makes this set of equations different from the general set of mesoscale equation (2.1)-(2.5). Also, Recall that, for a function $h \in L^p(\mathbb{T}^2), 1 \le p \le \infty$, the mollification $\mathcal{J}_\epsilon h$ is defined as

$$\left(\mathcal{J}_\epsilon h\right)(x) = \frac{1}{\epsilon^2}\int_{\mathbb{T}^2} \phi\left(\frac{x-y}{\epsilon}\right) h(y)dy$$

with ϕ being a mollifier function such that $\phi \in C_0^\infty(\mathbb{T}^2), \phi \ge 0$ and $\int\limits_{\mathbb{T}^2} \phi dx = 1$.
Applying the Leray projection $\mathbb{P}$, one can rewrite the system (4.5) as

$$\begin{cases} \dfrac{d}{dt}\begin{pmatrix} U^\epsilon \\ \theta^\epsilon \end{pmatrix} = \dfrac{d}{dt}\vec{U}^\epsilon = F_\epsilon(\vec{U}^\epsilon), \\ \\ \vec{U}^\epsilon|_{t=0} = \begin{pmatrix} U_0 \\ \theta_0 \end{pmatrix} \end{cases} \tag{4.6}$$

where $\vec{U}^\epsilon = \begin{pmatrix} U^\epsilon \\ \theta^\epsilon \end{pmatrix} \in V^m(\mathbb{T}^2) \times H^m(\mathbb{T}^2)$ endowed with the norm

$$\|\vec{U}^\epsilon\|_{H^m} := \|U^\epsilon\|_{V^m} + \|\theta^\epsilon\|_{H^m}$$

and

$$F_\epsilon(\vec{U}^\epsilon) = \begin{pmatrix} F_\epsilon^1(\vec{U}^\epsilon) \\ \\ F_\epsilon^2(\vec{U}^\epsilon) \end{pmatrix} = \begin{cases} -\mathbb{P}\left[\mathcal{J}_\epsilon\left\{\left(\mathcal{J}_\epsilon U^\epsilon\right).\nabla\left(\mathcal{J}_\epsilon U^\epsilon\right)\right\}\right] + \mathbb{P}\left[\theta^\epsilon \hat{e}_2\right], \\ \\ -\mathcal{J}_\epsilon\left\{\left(\mathcal{J}_\epsilon U^\epsilon\right).\nabla\left(\mathcal{J}_\epsilon \theta^\epsilon\right)\right\} + \mathcal{J}_\epsilon\{\left(\mathcal{J}_\epsilon \theta^\epsilon\right).\left(\mathcal{J}_\epsilon w^\epsilon\right)\}. \end{cases} \tag{4.7}$$

One can treat (4.6) as an ODE in the Banach space $V^m(\mathbb{T}^2) \times H^m(\mathbb{T}^2)$ with $F_\epsilon : V^m(\mathbb{T}^2) \times H^m(\mathbb{T}^2) \to V^m(\mathbb{T}^2) \times H^m(\mathbb{T}^2)$ as defined above in (4.7).

Lemma 5. *For $m > 1$, the functional $F_\epsilon : V^m(\mathbb{T}^2) \times H^m(\mathbb{T}^2) \to V^m(\mathbb{T}^2) \times H^m(\mathbb{T}^2)$ is locally Lipschitz.*

Proof. To show that $F_\epsilon(\vec{U}^\epsilon)$ is locally Lipschitz continuous, we estimate:

$$\begin{aligned} \|F_\epsilon^1(\vec{U}_1^\epsilon) - F_\epsilon^1(\vec{U}_2^\epsilon)\|_{H^m} &\leq C\| \left(\mathcal{J}_\epsilon U_1^\epsilon\right).\nabla\left(\mathcal{J}_\epsilon\left(U_1^\epsilon - U_2^\epsilon\right)\right)\|_{H^m} \\ &\quad + \| \left(\mathcal{J}_\epsilon\left(U_1^\epsilon - U_2^\epsilon\right)\right).\nabla\left(\mathcal{J}_\epsilon U_2^\epsilon\right)\|_{H^m} + \|\theta_1^\epsilon - \theta_2^\epsilon\|_{H^m} \\ &\equiv I + II + \|\theta_1^\epsilon - \theta_2^\epsilon\|_{H^m}. \end{aligned} \tag{4.8}$$

Using the following known estimates (see for example [26])

- For all $m \geq 0$, there exists $C > 0$ such that, for all $u, v \in L^\infty \cap H^m$,

$$\|uv\|_{H^m} \leq C\big(\|u\|_{L^\infty}\|D^m v\|_{L^2} + \|D^m u\|_{L^2}\|v\|_{L^\infty}\big) \tag{4.9}$$

$$\sum_{0\leq|\alpha|\leq m} \|D^\alpha(uv) - uD^\alpha v\|_{L^2} \leq C\{\|\nabla u\|_{L^\infty}\|D^{m-1}v\|_{L^2} + \|D^m u\|_{L^2}\|v\|_{L^\infty}\} \tag{4.10}$$

  where $D^\alpha(\cdot) = \partial_1^{\alpha_1}\partial_2^{\alpha_2}\cdots\partial_n^{\alpha_n}(\cdot)$ with $\alpha = (\alpha_1, \alpha_2, \cdots, \alpha_n)$, and $D^m = \sum_{\alpha\leq m} D^\alpha$.

- For all $v \in H^m, k \geq 0$, and $\epsilon > 0$,

$$\|\mathcal{J}_\epsilon v\|_{m+k} \leq \frac{C_{mk}}{\epsilon^k}\|v\|_{H^m}, \tag{4.11}$$

one can estimate the terms in (4.8) as

$$
\begin{aligned}
I \quad &\equiv \quad \| \left(\mathcal{J}_\epsilon U_1^\epsilon\right).\nabla \left(\mathcal{J}_\epsilon \left(U_1^\epsilon - U_2^\epsilon\right)\right) \|_{H^m} \\
&\overset{Using\,(4.9)}{\leq} \quad C\{\|\mathcal{J}_\epsilon U_1^\epsilon\|_{L^\infty} \|D^m \nabla \mathcal{J}_\epsilon \left(U_1^\epsilon - U_2^\epsilon\right)\|_{L^2} + \|D^m \mathcal{J}_\epsilon U_1^\epsilon\|_{L^2} \|\nabla \mathcal{J}_\epsilon \left(U_1^\epsilon - U_2^\epsilon\right)\|_{L^\infty}\} \\
&\overset{m>1,(4.11)}{\leq} \quad C\{\|\mathcal{J}_\epsilon U_1^\epsilon\|_{H^m} \|D^{m+1} \mathcal{J}_\epsilon \left(U_1^\epsilon - U_2^\epsilon\right)\|_{L^2} + \|\mathcal{J}_\epsilon U_1^\epsilon\|_{H^m} \|\nabla \mathcal{J}_\epsilon \left(U_1^\epsilon - U_2^\epsilon\right)\|_{L^\infty}\} \\
&\overset{Using\,(4.11)}{\leq} \quad \frac{C}{\epsilon} \|U_1^\epsilon\|_{H^m} \|U_1^\epsilon - U_2^\epsilon\|_{H^m}.
\end{aligned}
$$

Using similar estimates as above, we can show that

$$
II \quad \leq \quad \frac{C}{\epsilon} \|U_2^\epsilon\|_{H^m} \| \left(U_1^\epsilon - U_2^\epsilon\right) \|_{H^m}.
$$

Therefore,

$$
\begin{aligned}
\|F_\epsilon^1(\vec{U}_1^\epsilon) - F_\epsilon^1(\vec{U}_2^\epsilon)\|_{H^m} \quad &\leq \quad C \left\{ \frac{1}{\epsilon} \|U_1^\epsilon\|_{H^m} \|U_1^\epsilon - U_2^\epsilon\|_{H^m} + \frac{1}{\epsilon} \|U_1^\epsilon - U_2^\epsilon\|_{H^m} \|U_2^\epsilon\|_{H^m} \right. \\
&\qquad \left. + \|\theta_1^\epsilon - \theta_2^\epsilon\|_{H^m} \right\} \\
&\leq \quad C \left(\frac{\|\vec{U}_1^\epsilon\|_{H^m}}{\epsilon}, \frac{\|\vec{U}_2^\epsilon\|_{H^m}}{\epsilon} \right) \|\vec{U}_1^\epsilon - \vec{U}_2^\epsilon\|_{H^m}
\end{aligned}
$$

Similarly,

$$
\|F_\epsilon^2(\vec{U}_1^\epsilon) - F_\epsilon^2(\vec{U}_2^\epsilon)\|_{H^m} \quad \leq \quad C \left(\frac{\|\vec{U}_1^\epsilon\|_{H^m}}{\epsilon}, \frac{\|\vec{U}_2^\epsilon\|_{H^m}}{\epsilon} \right) \|\vec{U}_1^\epsilon - \vec{U}_2^\epsilon\|_{H^m}
$$

Therefore, we can finally write that

$$
\|F_\epsilon(\vec{U}_1^\epsilon) - F_\epsilon(\vec{U}_2^\epsilon)\|_{H^m} \leq C \left(\frac{\|\vec{U}_1^\epsilon\|_{H^m}}{\epsilon}, \frac{\|\vec{U}_2^\epsilon\|_{H^m}}{\epsilon} \right) \|\vec{U}_1^\epsilon - \vec{U}_2^\epsilon\|_{H^m}
$$

showing that $F_\epsilon(\vec{U}^\epsilon)$ is locally Lipschitz continuous. □

From Cauchy-Lipschitz theorem, given $m > 1$, $\vec{U}_0 \in V^m(\mathbb{T}^2) \times H^m(\mathbb{T}^2)$ and $\epsilon > 0$, there exists a unique solution $\vec{U}^\epsilon \in C^1([\,0, T_\epsilon)\,; V^m(\mathbb{T}^2) \times H^m(\mathbb{T}^2))$. Now we show the local in time existence of smooth solutions for the system $(4.1) - (4.4)$.

Lemma 6. *Let $m > 2$ and $\vec{U}_0 \in V^m(\mathbb{T}^2) \times H^m(\mathbb{T}^2)$ for $m > 2$, then*

1. *$\vec{U}^\epsilon$ is uniformly bounded in $C([0,T];V^m(\mathbb{T}^2)\times H^m(\mathbb{T}^2))$ for some T with*

$$T=\frac{1}{C[1+\|\vec{U}(0)\|_{H^m}]}$$

2. *$\frac{\partial}{\partial t}\vec{U}^\epsilon$ is uniformly bounded in $C([0,T];V^{m-1}(\mathbb{T}^2)\times H^{m-1}(\mathbb{T}^2))$ for the above time T.*

Proof. Consider the first equation from equation (4.6):

$$\frac{\partial U^\epsilon}{\partial t}=-\mathbb{P}\left[\mathcal{J}_\epsilon\left\{\left(\mathcal{J}_\epsilon U^\epsilon\right).\nabla\left(\mathcal{J}_\epsilon U^\epsilon\right)\right\}\right]+\mathbb{P}\left[\theta^\epsilon\hat{e}_2\right]$$

Applying D^α with ($|\alpha|\le m$) to the above equation, then multiplying by $D^\alpha U^\epsilon$, integrating in x and using the identity (See for example [26])

$$\sum_{|\alpha|\le m}\int_{\mathbb{T}^2}\mathbb{P}\mathcal{J}_\epsilon\left[(\mathcal{J}_\epsilon U^\epsilon).\nabla D^\alpha(\mathcal{J}_\epsilon U^\epsilon)\right](D^\alpha U^\epsilon)=0,$$

we obtain

$$\begin{aligned}\frac{1}{2}\frac{d}{dt}\|U^\epsilon\|_{H^m}^2 &= -\sum_{|\alpha|\le m}\left\{\int_{\mathbb{T}^2}\mathbb{P}\left\{D^\alpha\left(\left(\mathcal{J}_\epsilon U^\epsilon\right).\nabla\left(\mathcal{J}_\epsilon U^\epsilon\right)\right)-\left(\left(\mathcal{J}_\epsilon U^\epsilon\right).\nabla D^\alpha\left(\mathcal{J}_\epsilon U^\epsilon\right)\right)\right\}\left(D^\alpha\mathcal{J}_\epsilon U^\epsilon\right)dx\right.\\ &\quad\left.+\int_{\mathbb{T}^2}D^\alpha\left[\mathbb{P}\left\{\theta^\epsilon\hat{e}_2\right\}\right]\left(D^\alpha U^\epsilon\right)dx\right\}\\ &\overset{(4.10)}{\le} C\left\{\|\nabla\left(\mathcal{J}_\epsilon U^\epsilon\right)\|_{L^\infty}\|U^\epsilon\|_{H^m}+\|U^\epsilon\|_{H^m}\|\nabla\left(\mathcal{J}_\epsilon U^\epsilon\right)\|_{L^\infty}\right\}\|U^\epsilon\|_{H^m}\\ &\quad+\ \|\theta^\epsilon\|_{H^m}\|U^\epsilon\|_{H^m}.\end{aligned}$$

That is

$$\frac{d}{dt}\|U^\epsilon\|_{H^m}\le C\left\{1+\|\nabla\left(\mathcal{J}_\epsilon\vec{U}^\epsilon\right)\|_{L^\infty}\right\}\|\vec{U}^\epsilon\|_{H^m}. \tag{4.12}$$

Similarly, we can show that

$$\frac{d}{dt}\|\theta^\epsilon\|_{H^m}\le C\left\{\|\nabla\left(\mathcal{J}_\epsilon\vec{U}^\epsilon\right)\|_{L^\infty}\right\}\|\vec{U}^\epsilon\|_{H^m}+\|\vec{U}^\epsilon\|_{H^m}^2 \tag{4.13}$$

In deriving the above equation (4.13), the estimate of the nonlinear term $\mathcal{J}_\epsilon\{(\mathcal{J}_\epsilon\theta^\epsilon).(\mathcal{J}_\epsilon w^\epsilon)\}$

is evaluated as follows:

$$\begin{aligned}
\sum_{|\alpha|\le m}\int_{\mathbb{T}^2} D^\alpha\left[\mathcal{J}_\epsilon\left\{(\mathcal{J}_\epsilon\theta^\epsilon)\quad(\mathcal{J}_\epsilon w^\epsilon)\right\}\right](D^\alpha\theta^\epsilon)\,dx& \\
&= \sum_{|\alpha|\le m}\int_{\mathbb{T}^2} D^\alpha\left[(\mathcal{J}_\epsilon\theta^\epsilon)(\mathcal{J}_\epsilon w^\epsilon)\right]D^\alpha(\mathcal{J}_\epsilon\theta^\epsilon)\,dx \\
&\le C\sum_{|\alpha|\le m}\|D^\alpha\left[(\mathcal{J}_\epsilon\theta^\epsilon)(\mathcal{J}_\epsilon w^\epsilon)\right]\|_{L^2}\cdot\|D^\alpha(\mathcal{J}_\epsilon\theta^\epsilon)\|_{L^2} \\
&\le C\|(\mathcal{J}_\epsilon\theta^\epsilon)(\mathcal{J}_\epsilon w^\epsilon)\|_{H^m}\cdot\|\mathcal{J}_\epsilon\theta^\epsilon\|_{H^m} \\
&\overset{(m>1)}{\le} C\left(\|\theta^\epsilon\|_{H^m}\|w^\epsilon\|_{H^m}\right)\|\theta^\epsilon\|_{H^m} \\
&\overset{(4.9)}{\le} C\left(\|\theta^\epsilon\|_{H^m}\|U^\epsilon\|_{H^m}\right)\|\theta^\epsilon\|_{H^m} \\
&\le C\|\vec{U}^\epsilon\|_{H^m}^2\|\theta^\epsilon\|_{H^m}
\end{aligned}$$

Using equations $(4.12)-(4.13)$ and the fact that $m>2$ (which helps us to avoid having the dependence on ϵ), we can write that $\|\nabla\left(\mathcal{J}_\epsilon\vec{U}^\epsilon\right)\|_{L^\infty}\le\|\vec{U}^\epsilon\|_{H^m}$ which helps us to further write that

$$\frac{d}{dt}\|\vec{U}^\epsilon\|_{H^m}\le C\left(1+\|\vec{U}^\epsilon\|_{H^m}\right)^2 \tag{4.14}$$

or,

$$\frac{d}{dt}\left(1+\|\vec{U}^\epsilon\|_{H^m}\right)\le C\left(1+\|\vec{U}^\epsilon\|_{H^m}\right)^2$$

which further gives us that

$$1+\|\vec{U}^\epsilon(t)\|_{H^m}\le\frac{1+\|\vec{U}(0)\|_{H^m}}{1-C\left[1+\|\vec{U}(0)\|_{H^m}\right]t}$$

which for $t\le T=\frac{1}{2C\left[1+\|\vec{U}(0)\|_{H^m}\right]}$ gives

$$\sup_{0\le t\le T}\|\vec{U}^\epsilon(t)\|_{H^m}\le 2\left[1+\|\vec{U}(0)\|_{H^m}\right]$$

The above estimate, which is uniform in time, shows that the solution to the regularized problem exists up to a $T=T\left(\|\vec{U}_0\|_{H^m}\right)>0$. A similar procedure leads to the

equation

$$\left\| \frac{d}{dt}\vec{U}^{\epsilon}(t) \right\|_{H^{m-1}} \leq \quad 2\|\vec{U}(0)\|^2_{H^m}$$

□

Using Aubin-Nitche Compactness Lemma [26], we can now pass to the limit to say that the limit function $\vec{U} \in C\left([0,T]; V^m\left(\mathbb{T}^2\right) \times H^m\left(\mathbb{T}^2\right)\right)$ satisfies the equation

$$\vec{U}_t = \begin{pmatrix} -\mathbb{P}\left(U.\nabla U\right) + \mathbb{P}\left(\theta \hat{e}_2\right) \\ \\ -\left(U.\nabla\theta\right) + \theta w \end{pmatrix}$$

and hence $\vec{U}$ is a solution to the equations $(4.1) - (4.4)$ (with normalized constants). To prove the uniqueness of the solution, we consider $\vec{U}_1$ and $\vec{U}_2$ as two different solutions to the equations $(4.1) - (4.4)$ with the same initial data and denote by $U = U_1 - U_2, \theta = \theta_1 - \theta_2$ and $p = p_1 - p_2$. This gives,

$$\frac{\partial U}{\partial t} + (U_1.\nabla)U + (U.\nabla)U_2 = -\nabla p + \theta \hat{e}_2 \tag{4.15}$$

$$\frac{\partial \theta}{\partial t} + (U_2.\nabla)\theta + (U.\nabla)\theta_1 = U\theta_1 + U_2\theta \tag{4.16}$$

Equation (4.15) further gives that

$$\frac{d}{dt}\|U\|_{L^2} \leq C\left(\|\vec{U}(0)\|_{H^m}\right)\|\vec{U}\|_{L^2}$$

and equation (4.16) implies that

$$\frac{d}{dt}\|\theta\|_{L^2} \leq C\left(\|\vec{U}(0)\|_{H^m}\right)\|\vec{U}\|_{L^2}.$$

Therefore,

$$\frac{d}{dt}\|\vec{U}\|_{L^2} \leq C\left(\|\vec{U}(0)\|_{H^m}\right)\|\vec{U}\|_{L^2}.$$

This finally implies that

$$\vec{U} = \begin{pmatrix} U \\ \theta \end{pmatrix} = 0$$

which proves the uniqueness of solutions and thus ends the proof of Theorem 1. □

In this section, we prove the nonlinear instability for the linear unstable mode constructed in 3. Before we proceed and present the main theorem regarding nonlinear instability, consider the following definition.

Definition 2. *Let $m > 0$, then a stationary solution $\vec{U}_{stat}$ of equations $(4.1) - (4.4)$ is said to be nonlinearly unstable, if there exists a positive constant $\delta_0 > 0$ such that for every arbitrary small $\delta > 0$, there exists a time $T_\delta > 0$ and a solution $U(t, x, z)$ of $(4.1) - (4.4)$ with the initial data $U(0, x, z)$ satisfying*

$$\|\vec{U}(0, x, z) - \vec{U}_{stat}\|_{H^m} \leq \delta$$

and

$$\|\vec{U}(T_\delta, x, z) - \vec{U}_{stat}\|_{L^2} \geq \delta_0.$$

and

$$\|\vec{U}(T_\delta, x, z) - \vec{U}_{stat}\|_{L^\infty} \geq \delta_0.$$

Now consider the main theorem of this chapter.

Theorem 2. *For $m > 2$, the stationary solution $\vec{U}_{stat}(z) = (u_0 \sin(z), 0, \theta_{stat})$ of equations $(4.1) - (4.4)$ is nonlinearly unstable in the sense of Definition 2.*

Remarks:

- The restriction of $m > 2$ is due to the well-posedness given in Theorem 1.
- Clearly, this instability also implies, in a classical way, the instability in higher space dimensions.

Proof. Rewriting the nonlinear set of equations $(4.1) - (4.4)$ (with normalized constants) in the form

$$\begin{cases} U_t + (U \cdot \nabla) U = -\nabla p + \theta \hat{e}_2, \\ \theta_t + (U \cdot \nabla) \theta = \hat{e}_2 \cdot U\theta, \\ \operatorname{div}(U) = 0 \end{cases} \tag{4.17}$$

Applying the Leray Projection $\mathbb{P}$ on (4.17) and decomposing $\vec{U}$ as

$$\vec{U} = \vec{U}_{stat} + \vec{U}'$$

the above system (4.17) can be written as

$$\vec{U}'_t + \mathcal{L}(\vec{U}') + \mathcal{Q}\left(\vec{U}', \nabla\vec{U}'\right) = 0,$$

where

$$\mathcal{Q}\left(\vec{U}', \vec{U}'\right) = \begin{cases} \mathbb{P}\left[\left(U' \cdot \nabla\right) U'\right], \\ \\ \left[\left(U' \cdot \nabla\right) \theta'\right] - \hat{e}_2 \cdot U'\theta' \end{cases}$$

and

$$\mathcal{L}(\vec{U}') = \begin{cases} \mathbb{P}\left[\left(U_{stat} \cdot \nabla\right) U' + \left(U' \cdot \nabla\right) U_{stat}\right] - \mathbb{P}\left[\theta'\hat{e}_2\right], \\ \\ \left[\left(U_{stat} \cdot \nabla\right) \theta' + \left(U' \cdot \nabla\right) \theta_{stat}\right] - \hat{e}_2 \cdot U'\theta_{stat} - \hat{e}_2 \cdot U_{stat}\theta'. \end{cases}$$

Construction of an approximate solution: The solution will be constructed using an iterative scheme similar to the one detailed in [27], let $\left(\sigma, \vec{U}_1\right)$ be the unstable solution to the linearized problem given by Lemma 1 and set

$$\vec{V}_1 = \vec{U}_1 e^{\Re(\sigma)t} = \begin{pmatrix} U_1 \\ \theta_1 \end{pmatrix} e^{\Re(\sigma)t} \tag{4.18}$$

Then, as the nonlinear term is quadratic, $\vec{U}_{stat} + \delta\vec{V}_1$ will solve a nonlinear problem with a remainder term (error) of order $\delta^2 e^{2\Re(\sigma)t}$. Now we construct a solution V_2 that solves the linear Cauchy problem

$$\begin{cases} \partial_t \vec{V}_2 + \mathcal{L}(\vec{V}_2) = \mathcal{R}_1(t) \\ \vec{V}_2 = 0 \ \text{ at } \ t = 0 \end{cases} \tag{4.19}$$

where $\mathcal{R}_1(t) = -Q(\vec{V}_1, \nabla\vec{V}_1)$ is the error term. As, $\mathcal{R}_1(t)$ is $O(\delta^2 e^{2t\mathcal{R}(\sigma)})$, then $\|\vec{V}_2(t)\|_{H^m}$ is $O(e^{2\Re(\sigma)t})$. Indeed, taking D^α spatial derivatives of equation (4.19), multiplying by $D^\alpha\vec{V}_2$ and integrating, we get the following identity

$$\frac{d}{dt}\|\vec{V}_2(t)\|_{H^m} \leq C_1\|\vec{V}_2(t)\|_{H^m} + C_2\left(\|\vec{U}_1\|_{H^m}\right) e^{2\Re(\sigma)t}$$

or,

$$\|\vec{V}_2(t)\|_{H^m} \leq C_2\left(\|\vec{U}_1\|_{H^m}\right) e^{2\Re(\sigma)t}.$$

Also, note that

$$\|\mathcal{R}_1(t)\|_{L^2} \leq C\left(\|\vec{U}_1\|_{H^m}\right) e^{2\Re(\sigma)t},$$

Inductively, defining the sequence $(V_n)_n$ by:

$$\begin{cases} \partial_t \vec{V}_{n+1} + \mathcal{L}(\vec{V}_{n+1}) = \mathcal{R}_n(t) \\ V_{n+1} = 0 \ \text{ at } \ t = 0 \end{cases}$$

and, by induction, one prove that

$$\|\vec{V}_{n+1}(t)\|_{H^m} \leq C_{n+1}\left(\|\vec{U}_1\|_{H^m}\right) e^{(n+1)\Re(\sigma)t}. \tag{4.20}$$

and

$$\|\mathcal{R}_n(t)\|_{L^2} \leq C\left(\|\vec{U}_1\|_{H^m}\right) e^{(n+1)\Re(\sigma)t},$$

where $\mathcal{R}_n(t) = -\sum_{k=1}^{n} Q(\vec{V}_k, \vec{V}_{n+1-k})$ is the error term. Indeed we know that $\|\vec{V}_n(t)\|_{H^m} \leq C_n\left(\|\vec{U}_1\|_{H^m}\right) e^{n\Re(\sigma)t}$, which implies that

$$\|\mathcal{R}_n(t)\|_{L^2} \leq C\left(\|\vec{U}_1\|_{H^m}\right) e^{(n+1)\Re(\sigma)t}.$$

To get the identity (4.20), we use the fact that $\mathcal{R}_n$ comprises of all $\vec{V}_{j'}s$ that are bounded in H^m for $j \leq n$ and proceed as in the proof of (4.14) using energy method. Now, one can construct an approximate solution of the form

$$\vec{V}^{app} \ = \ \vec{U}_{stat} + \sum_{j=1}^{N} \delta^j \vec{V}_j \tag{4.21}$$

with $\vec{V}^{app} = (V_U^{app}, V_\theta^{app})^T$. Observe that $\vec{V}_j = 0$ at $t = 0$ and

$$\|\vec{V}_j(t)\|_{H^m} \leq C_j\left(\|\vec{U}_1\|_{H^m}\right) e^{j\Re(\sigma)t}.$$

The value of N will shortly be fixed. Therefore, the regularity of $\vec{V}_j$ depends on the regularity of $\vec{U}_1$. The approximate solution (4.21) solves the equation

$$\vec{V}_t^{app} + \mathcal{Q}(\vec{V}^{app}, \nabla\vec{V}^{app}) = \mathcal{R}_{app}$$

where $\mathcal{R}_{app}(t)$ is the corresponding error of the approximate solution and it satisfies

$$\|\mathcal{R}_{app}(t)\|_{L^2} \leq C\delta^{N+1}e^{(N+1)\Re(\sigma)t}.$$

We can write that

$$\|\vec{V}^{app}(t) - \vec{U}_{stat}\|_{L^2} \geq C_1\delta e^{\Re(\sigma)t} - \sum_{j=2}^{N} C_j\delta^j e^{j\Re(\sigma)t}.$$

The above, with $T_\delta = \dfrac{1}{\Re(\sigma)}\log(1/\delta)$, can also be written as (for $t < T_\delta$)

$$\|\vec{V}^{app} - \vec{U}_{stat}\|_{L^2} \geq \frac{C_1\delta}{2}e^{\Re(\sigma)t}$$

Further, let $\vec{U}$ solve the nonlinear equation

$$\vec{U}_t + \mathcal{Q}\left(\vec{U}, \vec{U}\right) = 0$$

with initial data $\vec{U}_{stat} + \delta\vec{U}_1(0)$ and consider the difference $\vec{\xi} = (\xi_U, \xi_\theta)^T = \vec{U} - \vec{V}^{app}$. Then, $\vec{\xi}$ solves the equation

$$\vec{\xi}_t + \bar{\mathcal{Q}}(\vec{V}^{app}, \vec{\xi}) + \mathcal{Q}(\vec{\xi}, \vec{\xi}) = -\mathcal{R}_{app}. \tag{4.22}$$

Here

$$\bar{\mathcal{Q}}(\vec{V}^{app}, \vec{\xi}) = \begin{cases} \mathbb{P}\left[(V_U^{app}\cdot\nabla)\,\xi_U + (\xi_U\cdot\nabla)\,V_U^{app}\right], \\ \\ (V_U^{app}\cdot\nabla)\,\xi_\theta + (\xi_U\cdot\nabla)\,V_\theta^{app} - \hat{e}_2\cdot\xi_U V_\theta^{app} - \hat{e}_2\cdot V_U^{app}\xi_\theta \end{cases}$$

From the above equation (4.22), we get

$$\frac{d}{dt}\|\vec{\xi}(t)\|_{L^2} \leq \left[\|\nabla\vec{V}^{app}(t)\|_{L^\infty} + C\right]\|\vec{\xi}(t)\|_{L^2} + \|\mathcal{R}_{app}(t)\|_{L^2}$$

as long as $\|\nabla\vec{V}^{app}(t)\|_{L^\infty}$ is finite, writing the above equation as (with $\tilde{C} = \|\nabla\vec{V}^{app}\|_{L^\infty} + C$)

$$\frac{d}{dt}\|\vec{\xi}(t)\|_{L^2} \leq \tilde{C}\|\vec{\xi}(t)\|_{L^2} + \|\mathcal{R}_{app}(t)\|_{L^2},$$

which further implies that

$$\begin{aligned}
\|\vec{\xi}(t)\|_{L^2} &\leq \int_0^t e^{\tilde{C}(t-s)}\|\mathcal{R}_{app}(s)\|_{L^2}ds \\
&\leq C\delta^{N+1}e^{\tilde{C}t}\int_0^t e^{\left[(N+1)\Re(\sigma)-\tilde{C}\right]s}ds \\
&= \frac{C\delta^{N+1}e^{\tilde{C}t}}{(N+1)\Re(\sigma)-\tilde{C}}\left[e^{[(N+1)\Re(\sigma)-\tilde{C}]t}-1\right]
\end{aligned}$$

or

$$\|\vec{\xi}(t)\|_{L^2} \leq \frac{C}{(N+1)\Re(\sigma)-\tilde{C}}\delta^{N+1}e^{(N+1)\Re(\sigma)t} \tag{4.23}$$

for sufficiently large N, such that $(N+1)\Re(\sigma) > \tilde{C}$. Therefore, finally, for $t = T_0 - \sigma_3$ with $\sigma_3 > \sigma_1$, we can write

$$\|\vec{U}-\vec{U}_{stat}\|_{L^2} \geq \|\vec{V}^{app}-\vec{U}_{stat}\|_{L^2} - \|\vec{\xi}\|_{L^2} \geq \frac{1}{2}e^{-\Re(\sigma)\sigma_3}\left[1-\frac{2Ce^{-N\Re(\sigma)\sigma_3}}{(N+1)\Re(\sigma)-\tilde{C}}\right] = \delta_0$$

where δ_0 does not depend on δ. As the $L^\infty(\mathbb{T}^2)$ norm controls the $L^2(\mathbb{T}^2)$ norm, the above estimate also holds for $L^\infty(\mathbb{T}^2)$. This completes the proof of the main Theorem 2. □

Chapter 5

Another Numerical Scheme Tried

Other than the numerical scheme mentioned in section-2.3.1, we spent quite a lot of time trying to solve the governing linear set of equations using the Laplace and the Fourier transforms. The idea was first to solve the governing set of equations by transforming them into the Laplace (for t) and Fourier (for x) spaces and then to use the numerical inversion of the Laplace transform and the well known Inverse Fast Fourier transform (IFFT) to get the results in the physical space. As the IFFT is a well known technique, we didn't have any trouble with that either. However, we noticed that the performance of the numerical inversion of the Laplace transform was very bad and had serious issues with it. In the coming sections in this chapter, we show some examples of the transform pairs, both for the numerical inversion of the Laplace and the IFFT to discuss their performance.

5.1 Numerical Inversion of the Laplace Transform

Recall that the Laplace transform $F(s)$ of a function $f(t)$ is defined by the integral

$$F(s) = \int_0^\infty e^{-st} f(t) dt, \qquad s \in \mathbb{C} \tag{5.1}$$

Whereas, the Inverse Laplace transform is defined by the following contour integral

$$f(t) = \frac{1}{2i\pi} \lim_{T \to \infty} \int_{\sigma - iT}^{\sigma + iT} F(s) e^{st} ds. \tag{5.2}$$

Here, the variable of integration is $s = \sigma + iT$. Following assumptions are considered on $F(s)$:

- $F(s)$ is regular for $\mathbf{Re}\{s\} > 0$.
- $\lim_{|s|\to 0} F(s) = 0$.
- $F^*(s) = F(s^*)$.

For the numerical inversion of Laplace transform, we implemented the scheme presented in [28]. The scheme presented in [28] approximates the inverse Laplace integral (5.2) by approximating e^{st}. It introduces a parameter $a \gg \sigma t$ to write

$$e^{st} = \frac{e^a}{2\cosh(a - st)} = \frac{e^{st}}{1 + e^{-2a}e^{2st}} \tag{5.3}$$

Further, using the following series representations

$$\frac{1}{\cosh(z)} = 2\pi \sum_{n=0}^{\infty} \frac{(-1)^n \left(n + \frac{1}{2}\right)}{\left(n + \frac{1}{2}\right)^2 \pi^2 + z^2}, \tag{5.4}$$

$$\frac{1}{\sinh(z)} = \frac{1}{z} + 2z \sum_{n=1}^{\infty} \frac{(-1)^n}{n^2\pi^2 + z^2} \tag{5.5}$$

and then using the Cauchy residue theorem to evaluate the resulting contour integral, one can, respectively, obtain the following relations

$$f_c(t) = \frac{e^a}{t} \sum_{n=1}^{\infty} (-1)^n \mathbf{Im}\left\{F\left[\frac{a}{t} + j\left(n - \frac{1}{2}\right)\frac{\pi}{t}\right]\right\} \tag{5.6}$$

$$f_s(t) = \frac{e^a}{t}\left[\frac{1}{2}F\left(\frac{a}{t}\right) + \sum_{n=1}^{\infty} (-1)^n \mathbf{Re}\left\{F\left(\frac{a}{t} + jn\frac{\pi}{t}\right)\right\}\right] \tag{5.7}$$

The MATLAB code that we implemented for numerical inversion of Laplace transform used the expression for $f_s(t)$. Further, to accelerate the convergence of the resulting series, [28] uses the Euler transformation. A parameter n_d is used to represent the number of added terms through the Euler transformation. Increasing n_d speeds up the process of convergence. So, we have three different parameters to deal with when using such an inversion of Laplace transform. The parameter a (in equation (5.7)), a parameter n_s which will represent the number of terms considered from the series

defined in equation (5.7) and the parameter n_d defined above. Now, let us consider some examples to test the convergence of the above method.

5.1.1 Examples for the Numerical Inversion of the Laplace transform

Consider the following examples of the Laplace transform pairs [29]:

$F_1(s) = \ln\left(\frac{s^2+4}{s^2}\right)$	$f_1(t) = \frac{2}{t}(1-\cos(2t))$

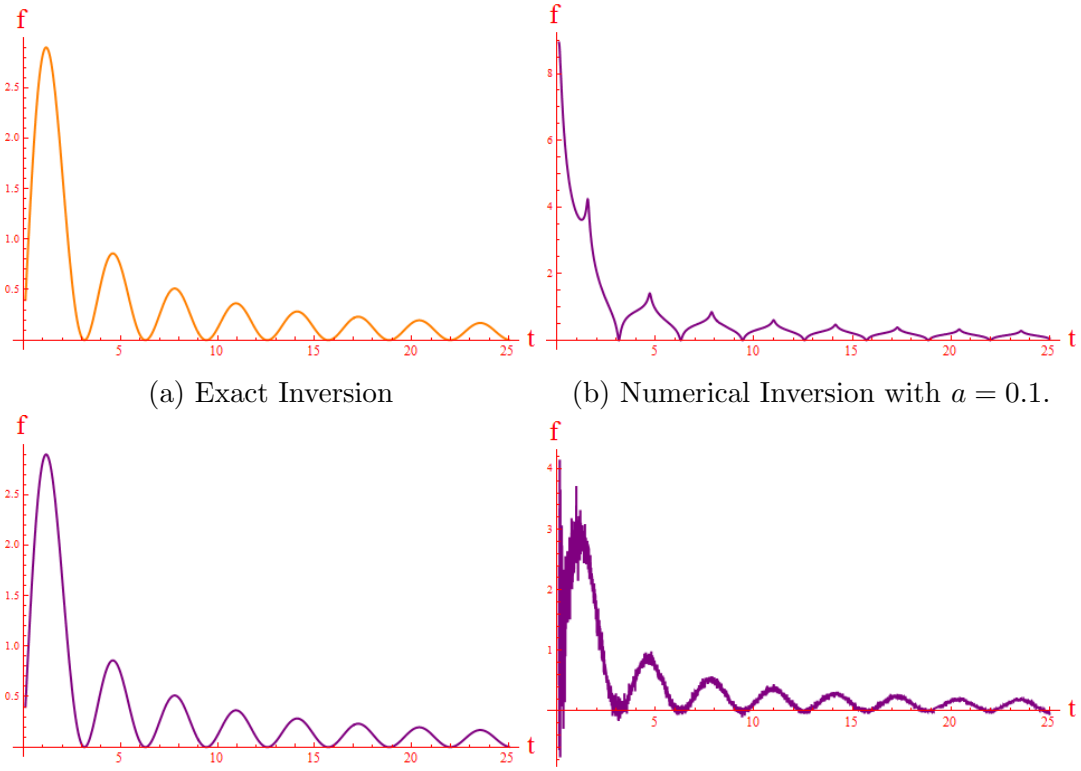

(a) Exact Inversion

(b) Numerical Inversion with $a = 0.1$.

(c) Numerical Inversion with $a = 20$.

(d) Numerical Inversion with $a = 34$.

Figure 5.1: Comparison of exact inversion of the Laplace transform of $F_1(s)$ with the Numerical Inversion of the Laplace transform for different values of the parameter a and with $n_s = 50$ and $n_d = 49$.

$F_2(s) = \dfrac{s}{s^2+4}$	$f_2(t) = \cos(2t)$

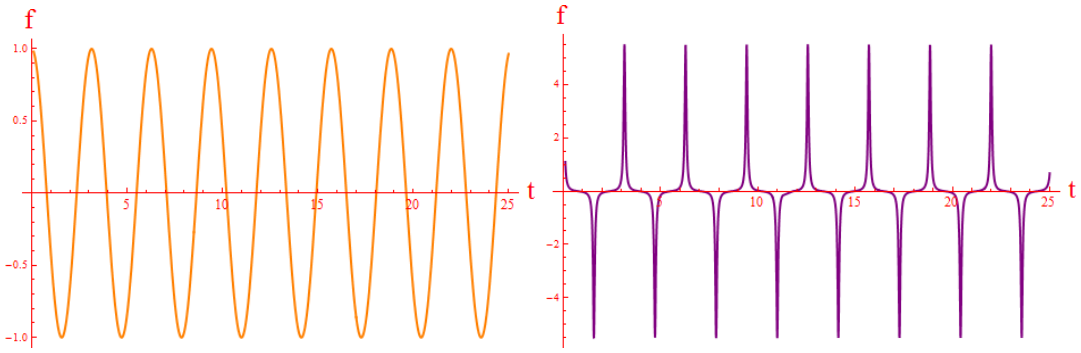

(a) Exact Inversion (b) Numerical Inversion with $a = 0.1$.

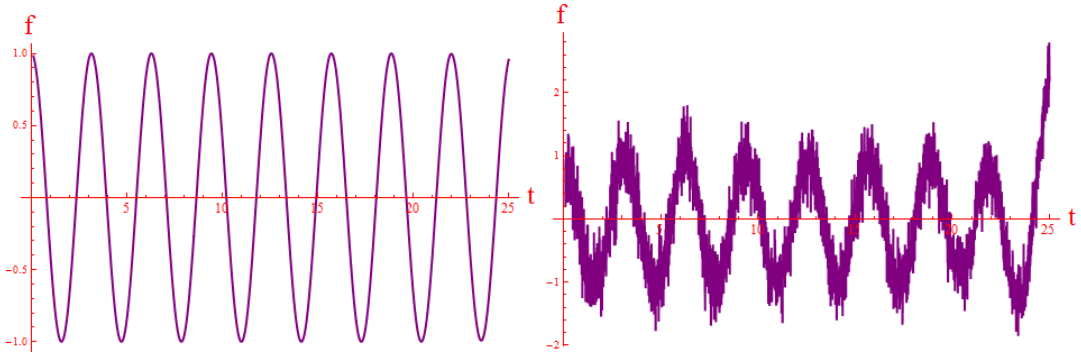

(c) Numerical Inversion with $a = 20$. (d) Numerical Inversion with $a = 38$.

Figure 5.2: Comparison of exact inversion of the Laplace transform of $F_2(s)$ with the Numerical Inversion of the Laplace transform for different values of the parameter a and with $n_s = 50$ and $n_d = 49$.

$F_3(s) = \dfrac{1}{\sqrt{s^2+4}}$	$f_3(t) = J_0(2t)$

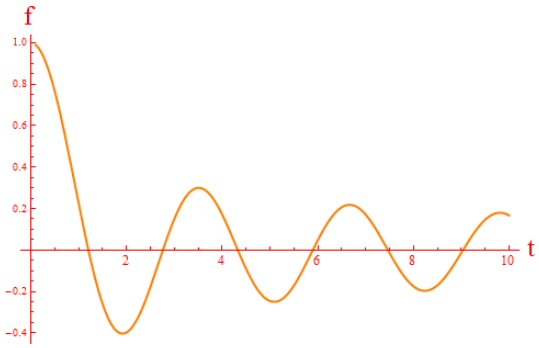

(a) Exact Inversion

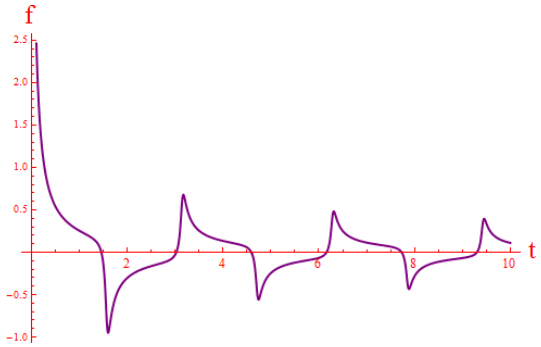

(b) Numerical Inversion with $a = 0.1$.

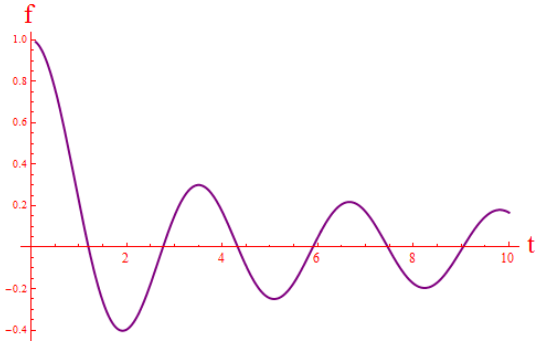

(c) Numerical Inversion with $a = 10$.

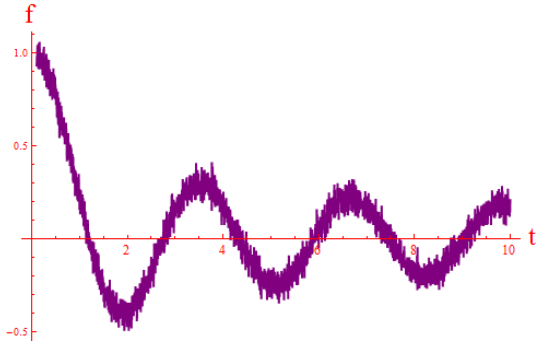

(d) Numerical Inversion with $a = 36$.

Figure 5.3: Comparison of exact inversion of the Laplace transform of $F_3(s)$ with the Numerical Inversion of the Laplace transform for different values of the parameter a and with $n_s = 50$ and $n_d = 49$.

$F_4(s) = erf\left(\frac{2}{\sqrt{s}}\right)$	$f_4(t) = \frac{1}{\pi t}\sin\left(4\sqrt{t}\right)$

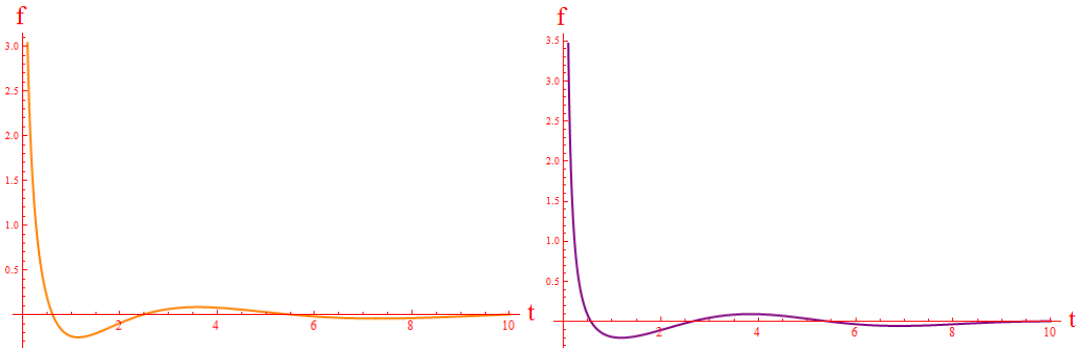

(a) Exact Inversion (b) Numerical Inversion with $a = 0.1$.

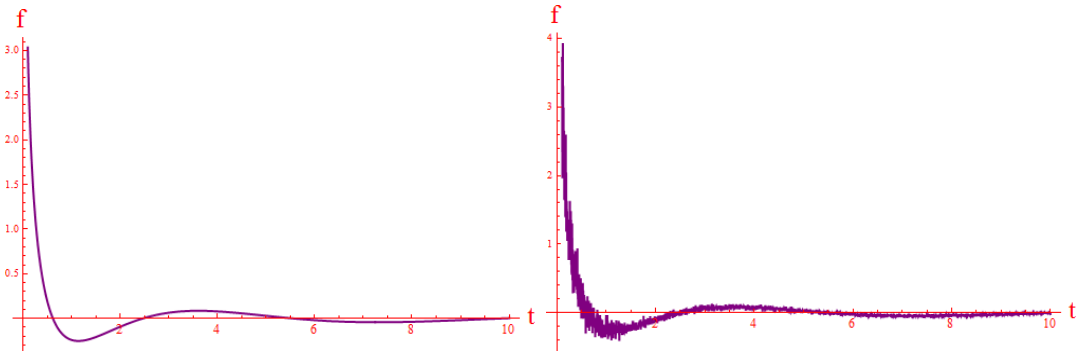

(c) Numerical Inversion with $a = 10$. (d) Numerical Inversion with $a = 32$.

Figure 5.4: Comparison of exact inversion of the Laplace transform of $F_4(s)$ with the Numerical Inversion of the Laplace transform for different values of the parameter a and with $n_s = 80$ and $n_d = 79$.

$F_5(s) = \dfrac{e^{-2\sqrt{s}}}{\sqrt{s}}$	$f_5(t) = \frac{1}{\pi t} e^{-1/t}$

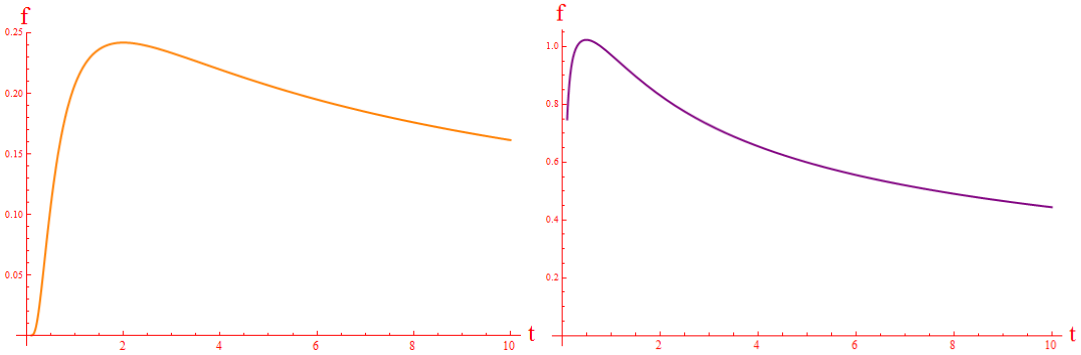

(a) Exact Inversion (b) Numerical Inversion with $a = 0.1$.

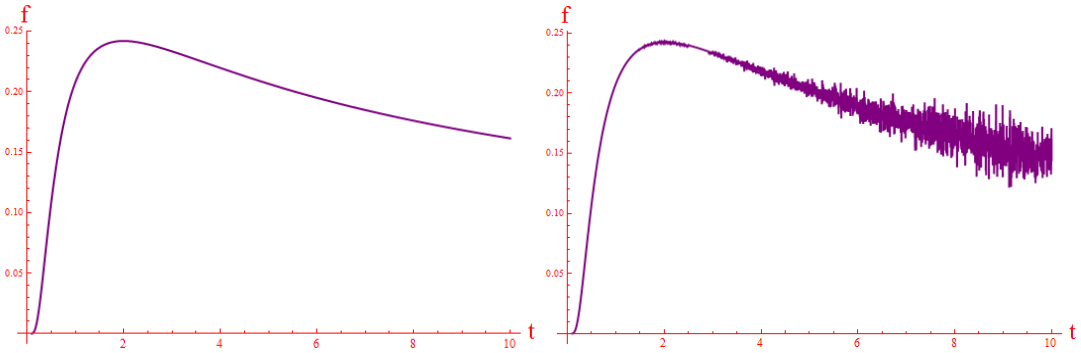

(c) Numerical Inversion with $a = 10$. (d) Numerical Inversion with $a = 37$.

Figure 5.5: Comparison of exact inversion of the Laplace transform of $F_5(s)$ with the Numerical Inversion of the Laplace transform for different values of the parameter a and with $n_s = 70$ and $n_d = 79$.

$F_6(s) = \frac{e^{2s}}{s} K_1(2s)$	$f_6(t) = \frac{1}{2}\sqrt{t(t+4)}$

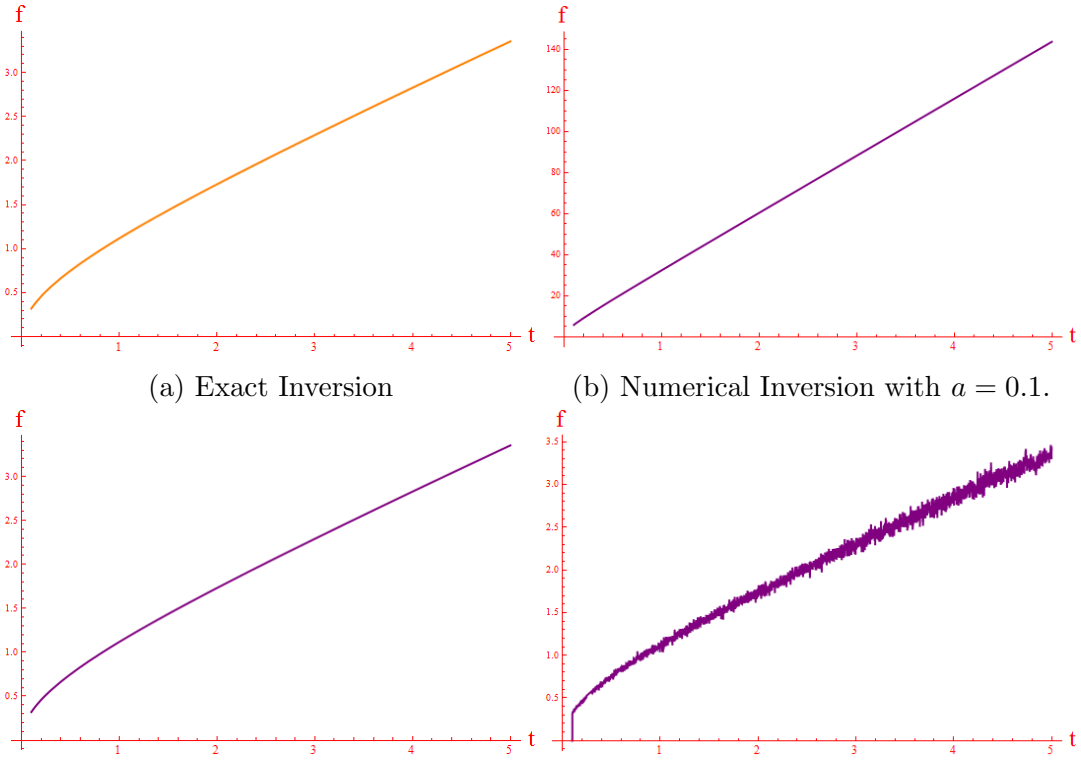

(a) Exact Inversion

(b) Numerical Inversion with $a = 0.1$.

(c) Numerical Inversion with $a = 20$.

(d) Numerical Inversion with $a = 37$.

Figure 5.6: Comparison of exact inversion of the Laplace transform of $F_6(s)$ with the Numerical Inversion of the Laplace transform for different values of the parameter a and with $n_s = 70$ and $n_d = 79$.

So, n_d, n_s and a are the parameters that we need to vary. When we find the solution to the governing equations in the Laplace space, we run into very complicated and tedious expressions. In such cases, plotting the solutions can cause serious problems. Also, to get the convergence of the numerical solutions with respect to the parameter a is a serious issue with this numerical algorithm. The strength of the contours increases to infinity as a increases. However, the algorithm itself suggests that bigger the value of a is, the better the approximation should be. Also, the number of terms considered n_s and the parameter n_d play a vital role as well. For better convergence, we need larger values of n_s and n_d which makes the method a lot more time consuming.

5.2 Inverse Fourier Transform

The continuous Fourier transform $\hat{f}(\omega)$ of $f(x)$ is given as

$$\hat{f}(\omega) = \int_{-\infty}^{\infty} e^{-2i\pi\omega x} f(x) dx \tag{5.8}$$

and the continuous Inverse Fourier transform is given as

$$f(x) = \frac{1}{2\pi} \int_{-\infty}^{\infty} e^{2i\pi\omega x} \hat{f}(\omega) d\omega \tag{5.9}$$

5.2.1 Relationship between Continuous Fourier transform and Discrete Fourier transform

Considering

$$f_k = k\tau, \qquad f_k = f(x_k), \qquad k = 0, 1, 2, ..., N-1 \tag{5.10}$$

where τ is the sampling interval. Now we approximate the continuous Fourier transform with a discrete sum, given as

$$\begin{aligned} \hat{f}(\omega) &= \int_{-\infty}^{\infty} e^{-2i\pi\omega x} f(x) \\ &\approx \sum_{k=-(N-1)}^{N-1} e^{-2i\pi\omega k\tau} f_k \tau \end{aligned} \tag{5.11}$$

Now taking $\omega = \frac{r}{N\tau}$, we get

$$\frac{1}{\tau}\hat{f}(\frac{r}{N\tau}) \approx \sum_{k=-(N-1)}^{N-1} e^{-\frac{2i\pi rk}{N}} f_k, \tag{5.12}$$

where

$$r = \frac{-N}{2}, ..., \frac{N}{2} \tag{5.13}$$

or

$$\frac{1}{\tau}\hat{f}(\frac{r}{N\tau}) \approx f^{DFT}(r). \tag{5.14}$$

with

$$f^{DFT}(r) = \sum_{k=-(N-1)}^{N-1} e^{-\frac{2i\pi rk}{N}} f_k \tag{5.15}$$

5.2.2 Examples for the Numerical Inversion of the Laplace transform

Now let us consider a few examples where we take the IFFT of the rescaled continuous Fourier transform of different functions in Matlab to check whether the result converges to the original function or not. Let us consider the following Fourier transform pairs (all with $\tau = 0.1$)

(1) $f(x) = e^{-|x|}$ with $\hat{f}(\omega) = \dfrac{2}{(2\pi\omega)^2 + 1}$

(a) $N = 30$

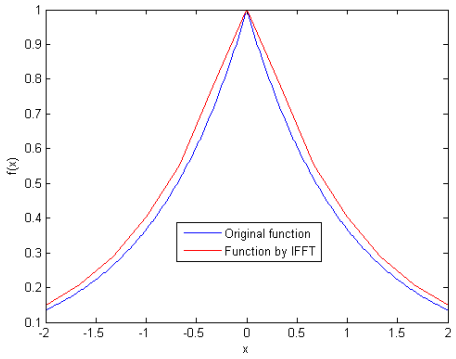

(b) $N = 70$s

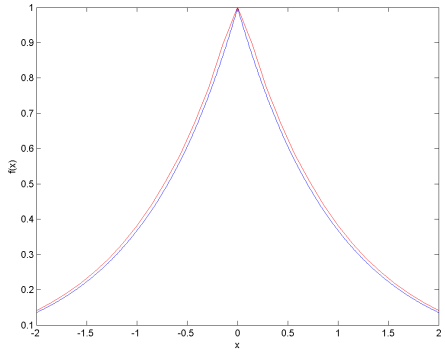

(c) $N = 120$s

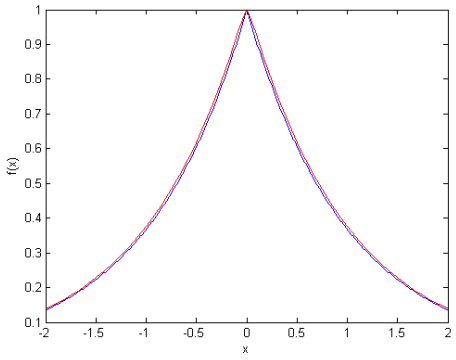

(d) $N = 200$ hour

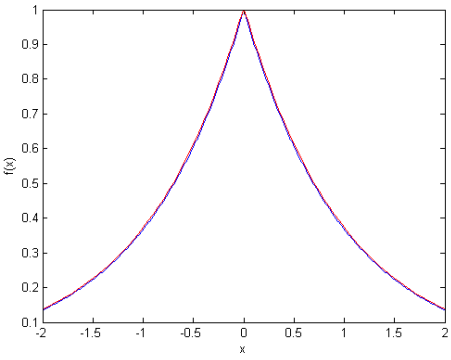

(2) $f(x) = e^{-x^2}$ with $\hat{f}(\omega) = \sqrt{\pi} e^{-\frac{\omega^2}{4}}$.

(e) $N = 30$

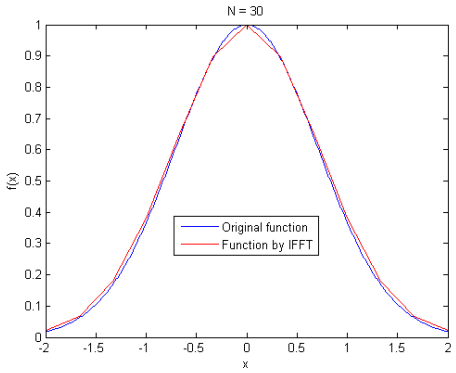

(f) $N = 70$s

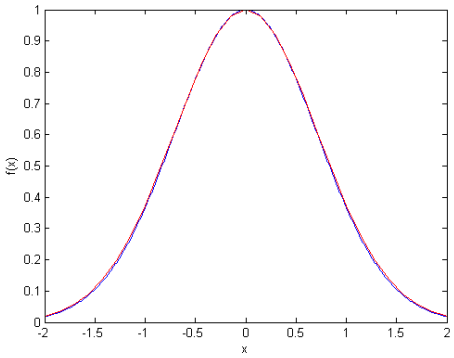

(g) $N = 120$s

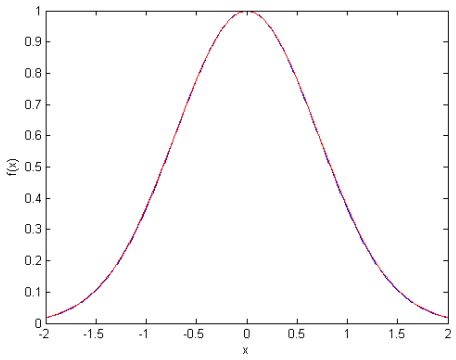

(h) $N = 200$ hour

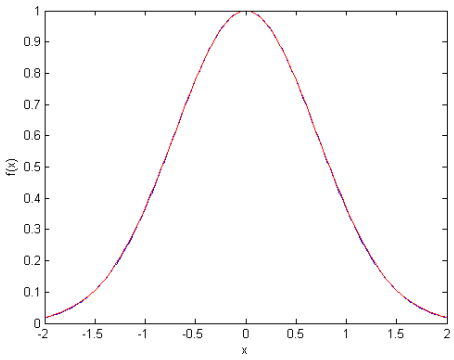

(3) $f(x) = \cos(2\pi\omega_0 x)$ with $\hat{f}(\omega) = \frac{1}{2}\left[\delta(\omega - \omega_0 + \delta(\omega - \omega_0))\right]$.

(i) $N = 30$

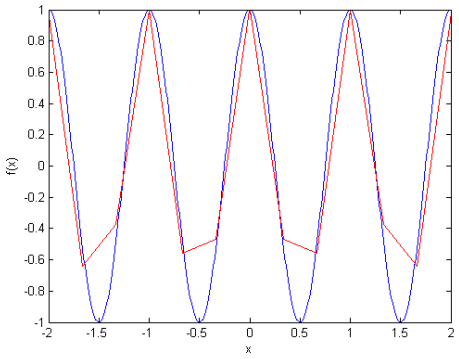

(j) $N = 70$s

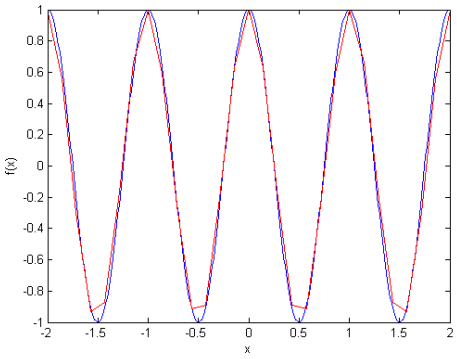

(k) $N = 120$s

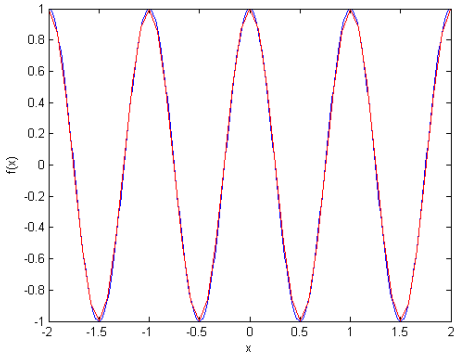

(l) $N = 200$ hour

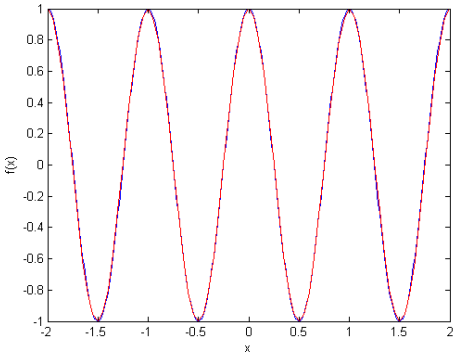

So, we can see that as we increase the value of N, or, as we increase the number of Fourier modes, we get closer and closer to the original function.

Chapter 6

Summary and Conclusion

In this dissertation, we considered the problem of a two dimensional, non-rotating and stably stratified mesoscale flow experiencing a thermal forcing. The considered thermal forcing was singular in time and space (only in the vertical). The dissertation was divided into two main parts. In the first part, a comparison between the hydrostatic and nonhydrostatic mesoscale processes was made to bring out the limitations of the hydrostatic assumption and to the best of our knowledge, such a comparison between the two cases for mesoscale equations experiencing a singular thermal forcing hasn't been previously made. In the second part of the dissertation, a smooth background profile was shown to be unstable for the set of nonlinear equations.

In order to make the comparison between the hydrostatic and nonhydrostatic cases, the governing set of nonlinear equations was initially linearized around a basic state profile. The flow was considered to be confined between two rigid layers, located at $z = 0$ and $z = 40$ Km. Periodic boundary conditions were considered along the horizontal direction and the computational domain was taken to be about 1000 Km. Further, the governing set of linearized equations was investigated under two different background profiles, namely, a constant background and a shear background profile. For hydrostatic cases, under both the background profiles, exact analytic solutions were used from [5, 6]. However, for nonhydrostatic cases, we used a fourth order filtered leap-frog scheme [12] to numerically simulate the governing set of linearized equations. The nonhydrostatic set of equations under zero background and a smooth sinusoidal forcing up to a height $z = L_z$ in the vertical direction were solved analytically [9] and numerically to validate our numerical code.

Under a uniform background profile, for short values of time, hydrostatic and nonhydrostatic cases were noticed to have some similarities in their behaviours but for large

values of time, the two cases came out completely different from each other, as shown in figures (2.2) and (2.3). After about half an hour, the symmetry of the contours, which was present in the hydrostatic case, was lost for the nonhydrostatic case. More significant differences between the two cases started to show up as time progressed further. Downwind propagating regions of upward and downward motions, that were observed for the nonhydrostatic case, were completely missing in the hydrostatic case. Similar observations for the shear background profile were deduced from figures (2.4) and (2.5). Further, to make sure that the differences in the behaviour of the two cases were not caused by the reflections from the top of the atmosphere considered, we added a 5 Km deep sponge layer of Rayleigh friction starting from 35 Km and ending at 40 Km in the vertical. The nonhydrostatic case maintained its differences from the hydrostatic one under both uniform and shear background profiles, even in the presence of sponge layer, as depicted by figures (2.6) and (2.7).

Lastly, we also included the nonlinearities in the system. Nonhydrostatic effects were found to be completely dominant over the effects of nonlinearities though. However, the splitting of the main moving mode that was observed by Han and Baik in [8] was also noticed in our case but only for very large (non-physical) values of the parameter ϕ that determined the strength of the nonlinearities. Our conjecture is, that the propagation of positive and negative regions in the nonhydrostatic case might represent waves of smaller-wavelength and as we move to the large scale dynamics (hydrostatic case) or equivalently to a larger-wavelength dynamics, this particular propagation is not observed any more.

In the second part of the thesis, we showed that a smooth sinusoidal background profile is nonlinearly unstable. To establish this result, as the diabatic heating considered previously was singular in time and space, we treated the forcing term differently in order to overcome some mathematical difficulties. We took the thermal forcing to be out of phase with the vertical component of the velocity which allowed the feedback of the atmosphere to the latent heating but with such a choice one may expect the instability to kick in if we increase the amplitude of the thermal forcing. Further, our consideration of the temperature T to be a constant and the replacement of the density ρ by the potential temperature θ in the buoyancy term made the governing set of nonlinear boussinesq equations different from the nonlinear mesoscale equations. Also, the domain for this part of the dissertation was considered to be the torus $\mathbb{T}^2$. This particular choice was again made to overcome some mathematical difficulties that arise while we try to establish the nonlinear instability for a linearly unstable

background profile.

Now, in order to prove the instability for the set of nonlinear equation, as an intermediate step, firstly, we show that the background profile $u_{stat} = u_0 \sin(z)$ is linearly unstable. To do so, we used the method of continued fractions which is restricted to the Torus, especially, in the $x-$direction. We also showed that for the governing set of linearized equations (zero forcing), a discontinuous background and a shear background profile that is linear in z within a layer in the vertical and constant outside, are unstable. In the later case, only longer wavelength waves were found to be unstable though. Secondly, we proved the well-posedness for the governing set of nonlinear equations. We established the well-posedness by first regularizing the system of equations and then further using the Cauchy-Lipschitz theorem and Aubin-Nitche Compactness Lemma [26], we were able to prove the local existence of solutions for the nonlinear problem. The nonlinear instability was then proven using the nonlinear iterative scheme introduced by Grenier [27].

As an example, with the diabatic heating having the form $q = \gamma w$, we were able to find an exact solution for the hydrostatic, linearized set of equations using an upper radiation and a mountain type boundary condition at the ground. It was observed that the solution stayed finite as long as the parameter γ stayed less than 1.

Finally, to conclude our work, we can state that for mesoscale flows under boussinesq approximations, hydrostatic assumption does not depict the complete dynamics, especially, for large values of time. Both under constant and shear background profiles, a downwind propagation of positive and negative regions was only observed in the nonhydrostatic case. The effect of nonlinearities were also found to be negligible as compared to the effect of nonhydrostaticity. Lastly, with the background profile being proportional to the vertical component of the velocity, a sinusoidal shear background profile is nonlinearly unstable.

Also, in the later part of this dissertation, while we were proving a smooth shear background profile to be unstable for the set of nonlinear equations, we made some non-physical assumption. Namely,

- Considering the diabatic forcing to be dependent on the vertical component of the velocity and taking the temperature T to be constant.
- Taking the domain to be periodic in the $z-$direction.
- Replacing the density ρ with potential temperature θ in the buoyancy term.

As these assumption are not physical, therefore, the nonlinear model that we worked with is one inspired by the general mesoscale model rather than being it. However, with the above mentioned limitations, this is a mathematical attempt to bring out some dynamical properties of the mesoscale flows. Therefore, removing the above mentioned non-physical restrictions and working with a more general physical mesoscale model will be a very interesting future direction for this kind of work.

Bibliography

[1] Y. L. Lin. *Mesoscale Dynamics*. Cambridge University Press, 2007.

[2] Paul Markowski and Yvette Richardson. *Mesoscale Meteorology in Midlatitudes*. John Wiley & Sons, 2010.

[3] James R. Holton. *An Introduction to Dynamic Meteorology*. Elsevier Academic Press, 2004.

[4] J. C. Jusem A. Barcilon and P. G. Drazin. On the two-dimensional, hydrostatic flow of a stream of moist air over a mountain ridge. *Geophys. Astrophys. Fluid Dyn.*, 13:125–140, 1979.

[5] J.-Y. Han and J.-J. Baik. Theoretical studies of convectively forced mesoscale flows in three dimensions. part i: Uniform basic-state flow. *J. Atmos. Sci.*, 66:947–965, 2009.

[6] Hong-Sub Hwang Jo-Jin Baik and Hye-Yeong Chun. Transient, linear dynamics of a stably stratified shear flow with thermal forcing and a critical level. *American Mathematical Society*, 15:483–499, 1999.

[7] JJi-Young Han and Jong-Jin Baik. Theoretical studies of convectively forced mesoscale flows in three dimensions. part ii: Shear flow with a critical level. *J. Atmos. Sci.*, 67:694–712, 2009.

[8] J.-Y. Han and J.-J. Baik. Nonlinear effects on convectively forced two-dimensional mesoscale flows. *J. Atmos. Sci.*, 69:3391–3404, 2012.

[9] M. Moustaoui. Mixing layer formation near the tropopause due to gravity wave-critical level interactions in a cloud-resolving model. *J. Atmos. Sci.*, 61:3112–3124, 2004.

[10] P. Queney. The problem of airflow over mountains: A summary of theoretical studies. *Bull. Amer. Meteor. soc.*, 29:16–26, 1948.

[11] T. L. Keller. Implications of the hydrostatic assumption on atmospheric gravity waves. *J. Atmos. Sci.*, 51(13):1915–1929, 1994.

[12] M. Moustaoui A. Mahalov, E. J. Kostelich. A numerical method based on leapfrog and a fourth-order implicit time filter. *American Mathematica Society*, pages 2545–2560, 2014.

[13] Ronald B. Smith and Yuh-Lang Lin. The addition of heat to a stratified airstream with application to the dynamics of orographic rain. *Quart. J. R. Met. Soc.*, 108:353–378, 1982.

[14] D. Bolton. Application of the miles theorem to forced linear perturbations. *J. Atmos. Sci.*, 37:1639–1642, 1980.

[15] L. N. Howard. Note on a paper of john miles. *J. Fluid Mech.*, 1961.

[16] L. Meshalkin and Y. Sinai. Investigation of stability for a system of equations describing plane motion of a viscous incompressible fluid. *Applied Math. and Mech.*, 25:1140–1143, 1961.

[17] Vincent Xiaosong Liu. Instability for the navier-stokes equations on the 2-dimensional torus and a lower bound for the hausdorff dimension of their global attractors. *Comm. Math. Phys.*, 147(2):217–230, 1992.

[18] S. Friedlander and V. Vicol. On the ill/well-posedness and nonlinear instability of the magneto-geostrophic equations. *Nonlinearity*, 24(11):3019–3042, 2011.

[19] W. Strauss S. Friedlander and M. Vishik. Nonlinear instability in an ideal fluid. *Ann. Inst. H. Poincare Anal. NonLineaire*, 14(2):187–209, 1997.

[20] W. Sun S. Friedlander, F. Gancedo and V. Vicol. On a singular incompressible porous media equation. *Journal of Mathematical Physics*, 2012.

[21] L.N. Howard P.G. Drazin. Hydrodynamic stability of parallel flow of inviscid fluid. *Advances in Applied Mechanics*, 1966.

[22] S. A. Thorpe. Neutral eigensolutions of the stability equation for stratified shear flow. *J. Fluid Mech.*, 1969.

[23] W. B. Jones and W. J. Thron. *Continued Fractions: Analytic theory and Applications, Encyclopedia of Mathematics and its Applications.* Addison-Wesley, 1980.

[24] A. Kacimi and B. Khouider. A numerical investigation of the barotropic instability on the equatorial beta-plane. *Theoretical and Computational Fluid Dynamics*, 27, Issue 3-4:491–512, 2013.

[25] Goldstein. On the stability of superposed streams of fluids of different densities. *Proc. R. Soc. Lond. A.*, 132:524–548, 1931.

[26] A. Bertozzi A. Majda. *Vorticity and Incompressible Flow.* 2001.

[27] Emmanuel Grenier. On the nonlinear instability of euler and prandtl equations. *Communications on Pure and Applied Mathematics*, LIII:1067–1091, 2000.

[28] Juraj Valsa and Lubomr Branik. A numerical investigation of the barotropic instability on the equatorial beta-plane. *International Journal of Numerical Modelling*, 11(3):153–166, 1998.

[29] Paul A. McCollum and Buck F. Brown. *Laplace Transform Tables and Theorems.* Holt, Rinehart and Winston, 1965.